ON THE ORIGIN OF THE LUNAR SMOOTH-PLAINS

V. R. OBERBECK
Space Science Division, NASA-AMES Research Center, Moffett Field, Calif., U.S.A.

F. HÖRZ
Planetary and Earth Sciences Division, NASA Johnson Space Center, Houston, Tex., U.S.A.

R. H. MORRISON
LFE Corporation, Richmond, Calif., U.S.A.

and

W. L. QUAIDE and D. E. GAULT
Space Science Division, NASA-AMES Research Center, Moffett Field, Calif., U.S.A.

(Received 4 July, 1974)

Abstract. Before the Apollo 16 mission, the material of the Cayley Formation (a lunar smooth plains) was theorized to be of volcanic origin. Because Apollo 16 did not verify such interpretations, various theories have been published that consider the material to be ejecta of distant multiringed basins. Results presented in this paper indicate that the material cannot be solely basin ejecta. If smooth-plains are a result of formation of these basins or other distant large craters, then the plains materials are mainly ejecta of secondary craters of these basins or craters with only minor contributions of primary-crater or basin ejecta. This hypothesis is based on synthesis of knowledge of the mechanics of ejection of material from impact craters, photogeologic evidence, remote measurements of surface chemistry, and petrology of lunar samples. Observations, simulations, and calculations presented in this paper show that ejecta thrown beyond the continuous deposits of large lunar craters produce secondary-impact craters that excavate and deposit masses of local material equal to multiples of that of the primary crater ejecta deposited at the same place. Therefore, the main influence of a large cratering event on terrain at great distances from such a crater is one of deposition of more material by secondary craters, rather than deposition of ejecta from the large crater.

Examples of numerous secondary craters observed in and around the Cayley Formation and other smooth plains are presented. Evidence is given for significant lateral transport of highland debris by ejection from secondary craters and by landslides triggered by secondary impact. Primary-crater ejecta can be a significant fraction of a deposit emplaced by an impact crater only if the primary crater is nearby. Other proposed mechanisms for emplacement of smooth-plains formations are discussed, and implications regarding the origin of material in the continuous aprons surrounding large lunar craters is considered. It is emphasized that the importance of secondary-impact cratering in the highlands has in general been underestimated and that this process must have been important in the evolution of the lunar surface.

1. Introduction

Interpretation of the nature and origin of the Cayley Formation at the Apollo 16 landing site is critical to understanding the geologic history of the Moon. It and other smooth plains of Imbrian age are widespread and predominantly occur in local depressions of most lunar highlands (see Figure 1). It was originally included in the Apenninian series with the hummocky deposits of Imbrium by Eggleton and Marshall (1962) because the hummocky deposits, exposed continuously southward from the Carpathian Mountains, become gradually smoother and seem to grade into a smooth,

The Moon **12** (1975) 19–54.

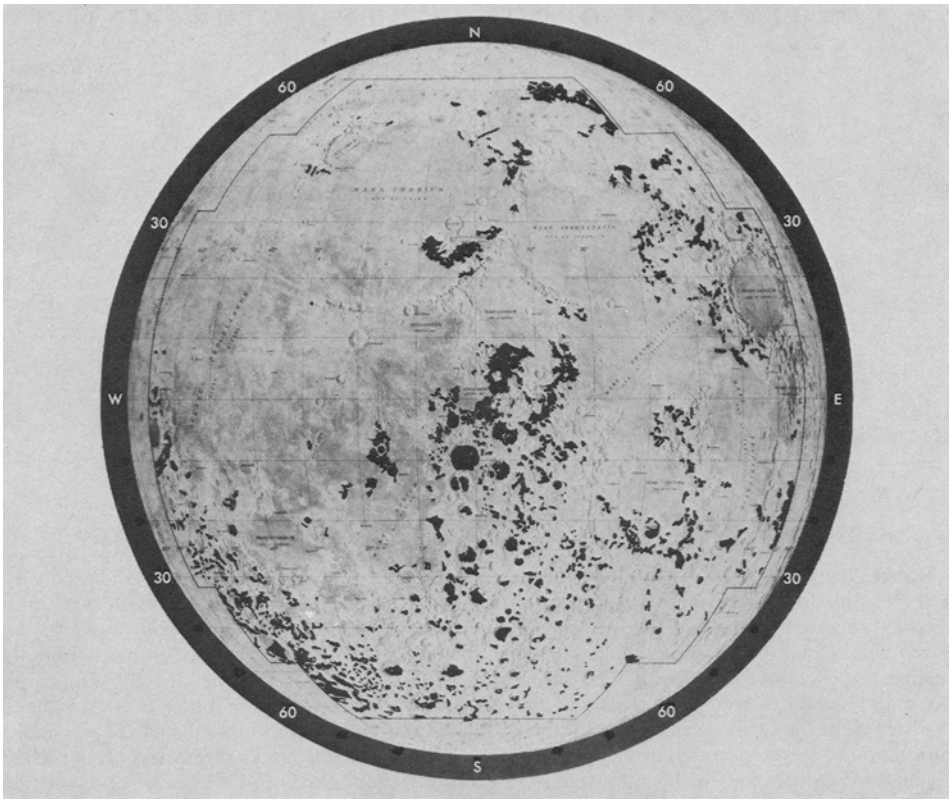

Fig. 1. Distribution of Imbrian smooth plains (indicated in black) on the lunar front side according to Wilhelms and McCauley (1971).

flat part without hummocks. Wilhelms (1965) separated this smooth facies from the hummocky Fra Mauro Formation and named it the Cayley Formation. Moreover, he noted that the outer contact of the smoothest facies of the Fra Mauro, next to the smoother Cayley Formation, was difficult to locate; maps of the Julius Caesar (Morris and Wilhelms, 1967) and Mare Vaporum quadrangles (Wilhelms, 1968) show some contacts between the smooth Fra Mauro and Cayley as questionable.

Local, sharp contacts of the Cayley Formation with adjacent rugged terrain, noted by Wilhelms (1965), suggest a considerable thickness of material in depressions (Figure 1). This, together with the common mantled appearance of the Cayley Formation, as deduced from muted forms of craters and other features, led to the conclusion that the formation might have been produced by volcanic processes (Wilhelms, 1965).

Volcanic concepts prevailed throughout the Apollo 16 premission interpretations, though many additional observations and interpretational details were added (Milton, 1972; Elston *et al.*, 1972; Wilhelms and McCauley, 1971; and Trask and McCauley, 1972). However, impact-generated breccias returned from the Apollo 16 landing site

failed to verify a volcanic origin for the Cayley Formation, at least at this particular locality. Analysis of the stratigraphy of North Ray crater and the block distribution at this site (Ulrich, 1973) have yielded a model for local stratification. A 50-m thick layer of light-colored, friable feldspathic impact breccias overlies more coherent, glass-rich dark-matrix impact breccias, containing as inclusions rocks of metaclastic and igneous appearance. Petrographic analyses of materials returned from many locations in the Apollo 16 Cayley plains reveal an exceptional variety of breccia types (LSPET, 1973; Warner *et al.*, 1973; Wilshire *et al.*, 1973; Walker *et al.*, 1973; Bence *et al.*, 1973, and others). Most of the returned rocks show evidence for multiple brecciation. All investigators emphasize that the highly complex multiple breccias imply a history of multiple-impact events and that the samples were exposed to elevated temperatures, either short of melting or with various degrees of partial melting. Such temperatures could have been induced by meteorite impact. Absolute formation ages between 3.8×10^9 and 4.24×10^9 yr for the Apollo 16 rocks (Tera *et al.*, 1973; Husain and Schaeffer, 1973; Compston *et al.*, 1973) imply discrete thermal (impact) events spanning this period.

Study of the magnetic properties of Apollo 16 rocks reveals that all rocks have very high metallic-iron content (Pearce *et al.*, 1973). In comparison with mare basalts such concentrations are interpreted to reflect severe thermal metamorphism of silicates in a highly reduced environment at temperatures above 770 °C, the Curie point of Fe. Thus, postmission analyses indicate that the Apollo 16 Cayley Formation consists of impact-generated breccias which exhibit a history of complex, multistage mechanical mixing and/or severe thermal metamorphism.

Any interpretation of emplacement of the Cayley Formation must therefore allow for exposure of the samples to impact of extralunar bodies before emplacement. Consequently, Chao *et al.* (1973), Hodges *et al.* (1973), and Eggleton and Schaber (1972) have proposed various mechanisms for emplacement of the formation from one or more distant impact basins. These mechanisms consider either all the materials or near surface materials of the Cayley Formation to be completely basin ejecta, transported to its present site in ballistic trajectories as ejecta or as fluidized debris from one or more large multiringed impact basins.

Results of laboratory simulation of impact of material in ballistic trajectories, coupled with computational results and observations of lunar craters and basins to be presented in this paper, show the smooth plains cannot be solely basin ejecta transported in ballistic trajectories. Ejecta of a large lunar crater transported beyond the crater's continuous deposits (which previously were assumed to be ejecta blankets) produce well-formed secondary craters that excavate and emplace much larger amounts of local material than primary-crater ejecta. Thus, if emplacement of the Cayley Formation and other smooth plains are related genetically to formation of large basins through ballistic transport, then they must consist mostly of ejecta of secondary craters of the basins rather than solely of basin ejecta. Therefore, previous hypotheses relating the smooth plains to formation of distant large basins must be revised to account for the role of secondary cratering associated with these basins.

Moreover, any revised hypothesis should account for the role of secondary cratering associated with nearby large highland craters in emplacement of the smooth plains.

Therefore a new hypothesis for emplacement of smooth plains of Imbrian and pre-Imbrian age is proposed: Many multiringed impact basins and other large impact craters ejected fragments to great distances on the Moon. The fragments impacting the higher elevations of the highlands produced secondary craters that ejected and deposited in the smooth-plains depressions masses of material many times greater than the mass of the fragments themselves. Also, nearby highland craters added to the smooth-plains areas significant amounts of primary-crater ejecta. However, even in this case, primary-crater ejecta eroded material from high elevations and deposited it along with primary-crater ejecta in local depressions in the highlands and floors of ancient craters where it reworked level areas. Efficient landslides triggered by secondary impact and secondary and small primary impacts in the plains areas effectively spread the eroded materials into large level plains, over a long period of time.

2. Effects of Ejection of Material from Large Lunar Impact Craters

2.1. Lunar secondary craters

Figure 2 shows a photomosaic of Copernicus crater and its surrounding terrain. Extending for hundreds of kilometers from this large crater is a striking system of rays which are due to concentrations of innumerable separated small secondary and tertiary craters having bright rock-strewn ejecta deposits (Oberbeck, 1971a). These craters were produced by impact of the lunar surface by ejecta of Copernicus (Oberbeck and Morrison, 1974), but the bright ejecta from secondaries and tertiaries consist mainly of local debris, not Copernican ejecta. Closer to Copernicus are relatively large secondary craters radiating from the primary crater in chains that are sometimes within bright rays. Some of these craters are only about 50 km from the rim of Copernicus. However, at points nearer to Copernicus no secondary craters are discernible because of the continuous deposits in this region; but this does not mean that secondary craters were not produced in this region during the cratering event.

Secondary craters are produced when fragments ejected from a crater impact the surface at velocities exceeding some critical velocity. This threshold velocity must be very low because secondary craters are present only 17 km from the rim of Euler crater. Moreover, although they are poorly developed, secondary craters are present only 0.6 km from the rim of a small mare crater, with diameter of 0.67 km, shown on Lunar Orbiter II, Frame No. 171, Site P-11-b, located at 0.24° W, 20.10° S. Therefore, in the case of Copernicus, secondary craters must have been produced even within the region of the continuous deposits; they are usually indiscernible because of the saturation of this region by numerous secondary craters. Therefore, primary-crater ejecta transported only a very short distance are capable of producing craters when they impact the surface. Because such craters excavate local materials even the continuous deposits of large basins should contain large amounts of local material in addition to basin ejecta. The maximum radial extent, R_{cd}, of the continuous deposits of craters

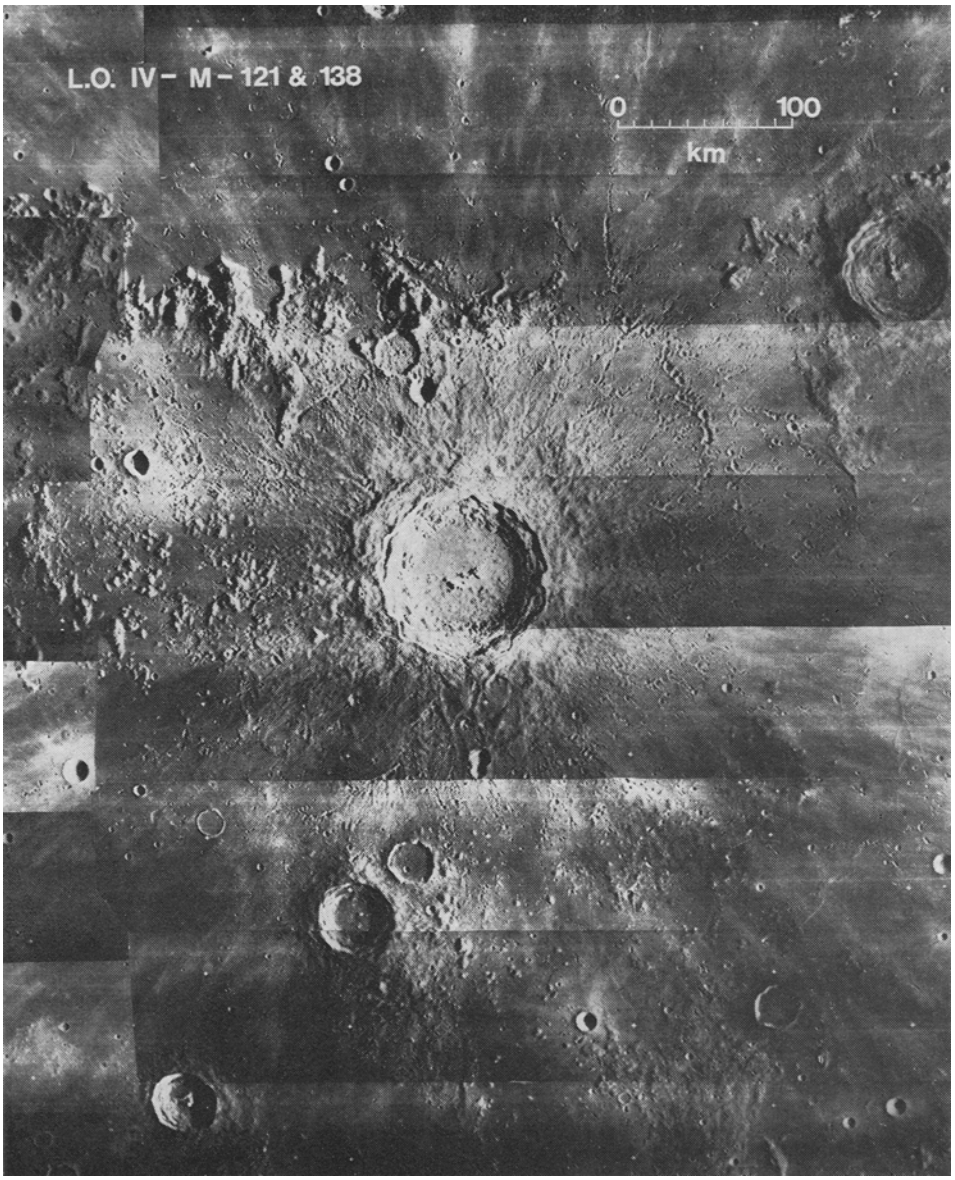

Fig. 2. Photomosaic of lunar crater Copernicus and associated ray pattern and secondary craters.

larger than 1 km can be taken as a conservative inner boundary for formation of separated secondary craters or crater chains. Estimates of this radius as a function of primary-crater radius, R_r, are given for several lunar craters and basins in Figure 3, which shows that the continuous crater-deposit radius varies nearly linearly with crater radius. Therefore, for any given primary crater in the size range from 3.5 to

1340 km in diameter, Figure 3 gives the radius of the boundary separating the region near the crater where the predominant effect of ejecta impacting the surface is to produce continuous deposits from the region far from the crater where the predominant effect is to produce well-developed secondary craters, provided material is ejected from the crater in a symmetrical or nearly symmetrical fashion.

Figure 4a shows a typical cluster of secondary craters of Copernicus located far from the outer boundary of the continuous deposits; the craters are all subdued, compared with similar-size primary craters. Those farthest from Copernicus are more subdued than those nearest. Moreover, those at the cluster's edge are typically more well-defined than those at the center. Figure 4b shows a secondary cluster that was probably produced by ejecta of Aristarchus crater. Those at the western edge of the chain are more defined as a group than those farthest from Aristarchus. The V-shaped ridges radiating from the crater chain are components of a lunar herringbone pattern (Oberbeck and Morrison, 1973, 1974). Because of the youthful appearance of the parent craters, these examples, although very subdued, must represent some of the freshest secondary craters on the Moon. Similar crater clusters and craters occur in great numbers around fresh, large lunar impact craters. Secondary craters of older primary craters are even more subdued. Thus, deposits emplaced by secondaries of large lunar craters and basins should contain large numbers of subdued craters.

Laboratory simulations indicate that secondary craters are subdued, at least partially, by simultaneous impact of fragments ejected from the parent crater. Figure 4c shows a plot of the ratio of h_D, the depth of the downrange crater, to h_U, the depth of the uprange crater, for crater pairs produced by simultaneous impact of two lexan

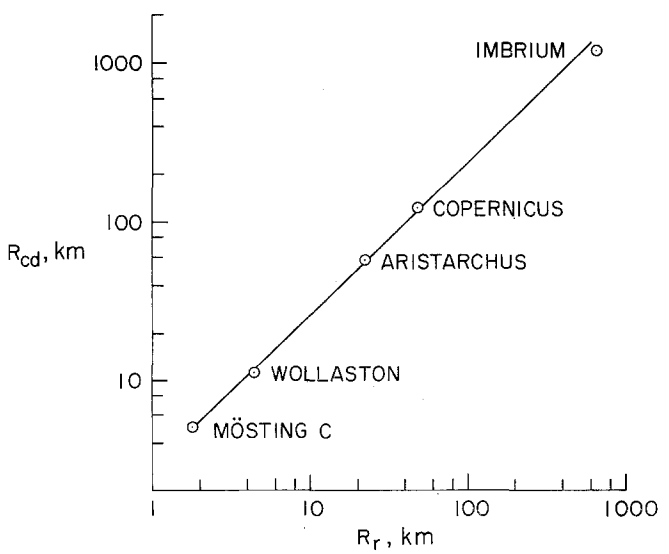

Fig. 3. Measured radius, R_{cd}, of continuous deposits around various lunar craters and basins as a function of crater or basin rim radius, R_r. For Imbrium, the radius of the continuous deposits (Short and Forman, 1972) is plotted vs the radius of the outer ring (Hartmann and Wood, 1971).

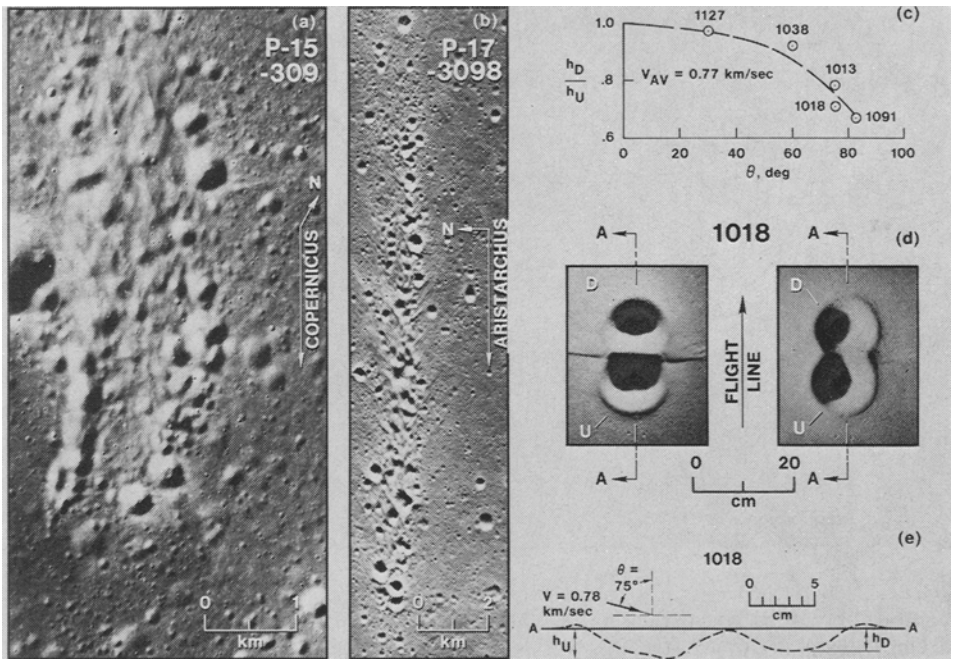

Fig. 4a–e. (a) Cluster of subdued secondary craters of Copernicus, located at 39°20′W, 28°15′N, approximately 151 km northeast of the center of Prinz crater. (b) Secondary craters of the crater Aristarchus, located at 27°0′W, 26°0′N, approximately 100 km northeast of the center of Euler crater. (c) Ratio of depth, h_D, of downrange crater to depth, h_U, of uprange crater for two craters produced simultaneously at various impact angles, θ. (d) Photographs of two craters produced in experiment 1018. (e) Profile along bilateral axis of symmetry for craters produced in experiment 1018.

projectiles of equal mass (0.43 g) into quartz sand at impact velocities and angles suitable for simulation of many lunar secondary craters (Oberbeck and Morrison, 1974). As impact angle, θ, measured from the normal increases, the ratio h_D/h_U decreases. Figure 4d shows two closely spaced craters (experiment 1018) produced simultaneously by projectiles impacting at a velocity of 0.78 km s^{-1} and impact angle of 75°. Their shadow patterns and crater-pair profile (Figure 4e) also show that the downrange crater is subdued most; ejecta from the uprange crater have partially filled the downrange crater. This probably explains the observation that lunar secondaries of a chain or cluster that are farthest from the parent crater are also the shallowest.

Secondary craters on slopes, being even more subdued than those on level terrain, are in many cases difficult to observe. Figure 5a shows an example: a large group of subdued (probable) Copernican secondaries superimposed on Delisle α, a high ridge northeast of Aristarchus, and on the surrounding level terrain. The crater field contains well-defined, though subdued craters, on each side of Delisle α, but not on the ridge slopes. Figure 5b shows another example: a secondary crater chain crossing a mare ridge. The group of craters indicated by the arrow nearest the ridge is almost com-

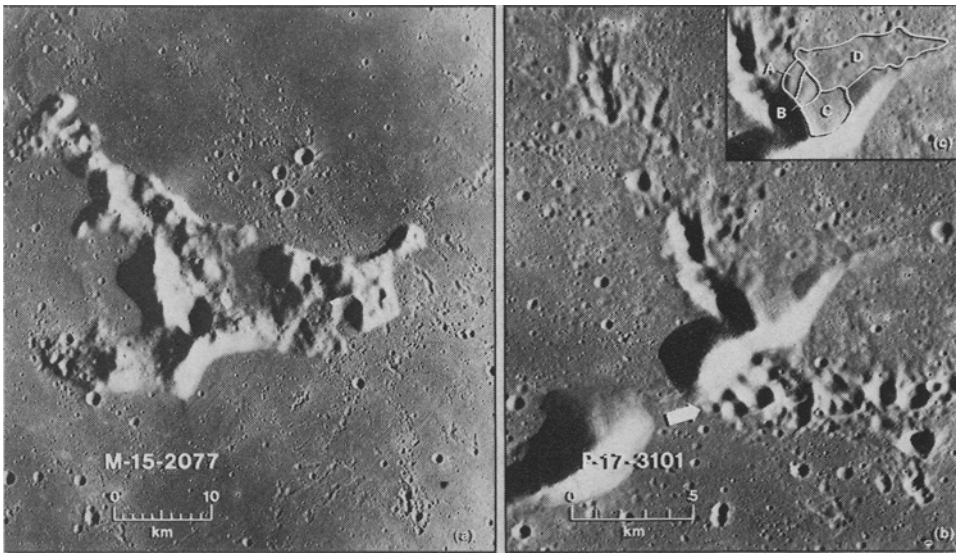

Fig. 5a–c. (a) Secondary craters that are visible on surface surrounding Delisle α but not on its high terrain. (b) Secondary crater chain crossing a mare ridge located at 27° 40′ W, 20° 40′ N, approximately 90 km southeast of the center of crater Euler. (c) Map of landslide caused by secondary craters of Figure 5b.

pletely filled, presumably by material dislodged from the ridge during impact. Thus, secondary craters are not well developed on slopes because slope materials are unstable and tend to slide; this in turn causes materials uphill from the craters also to become unstable and slide, obliterating the freshly produced craters. Thus, formation of secondaries on slopes adds material to depressions.

In summary, when ejecta of Copernicus impacted the surface they produced numerous secondary craters, some as close as 50 km from the crater's rim. Such craters, subdued even when newly formed, are poorly expressed on rugged terrain where they caused landslides of local material into depressions. However, secondary craters also can be produced by impact of material transported only very short distances. Few are observed in the continuous deposits of large craters, only because impact of their ejecta displaced local debris that swamped and filled any discrete craters that formed nearby (see also Wilhelms, 1965). However, for ejecta thrown beyond the continuous deposits of large primary craters (Figure 3), their spatial density is low enough to produce generally isolated craters or crater chains rather than continuous deposits.

In the following section, the mass of local material ejected from secondary craters is estimated and compared to primary-crater ejecta mass in several ways, but only for areas beyond the continuous deposits, where secondary craters or crater chains are separated from one another. Such calculations predict whether ejecta of large lunar craters transported a given distance will be deposited as a unit or whether such materials will be only a small part of the ejecta of secondary craters.

2.2. Mass ejected from secondary craters

2.2.1. *Ratio μ of Mass Ejected and Mass of Impacting Fragment*

Recent laboratory simulations indicate that secondary craters of Copernicus were formed by impact of fragments ejected from the crater at angles exceeding 60° measured from the normal (Oberbeck and Morrison, 1974). Moreover, the results of Shoemaker (1962) indicate a narrow range, from 68° to 76°, for these angles. To

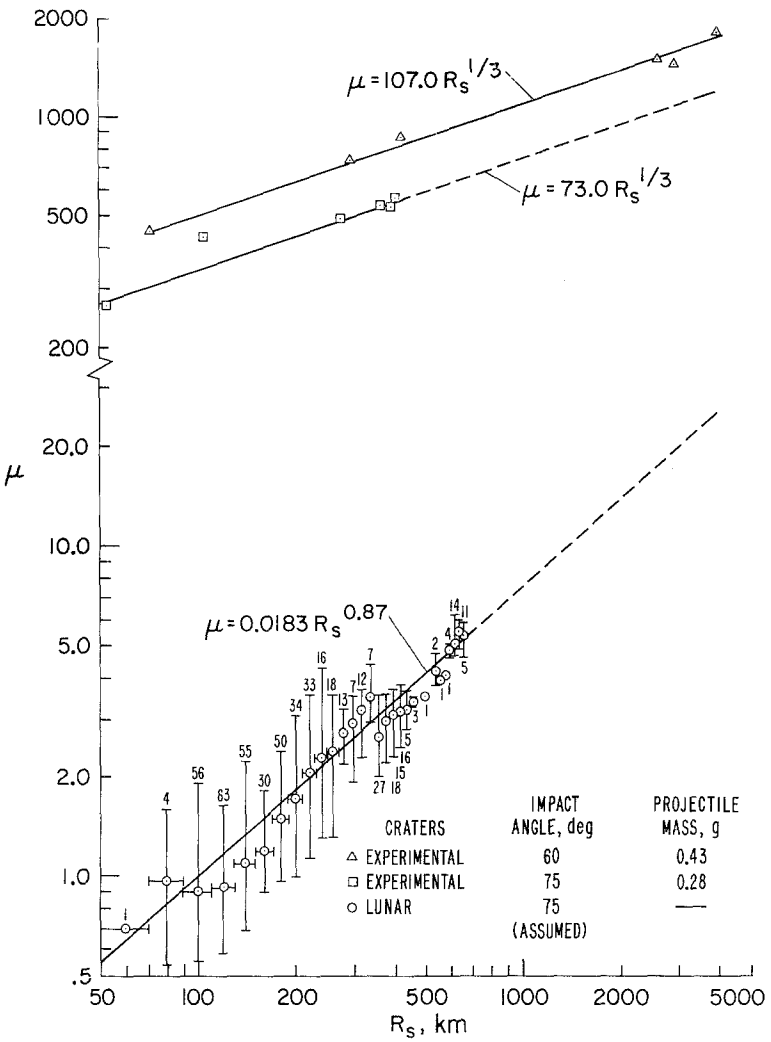

Fig. 6. Ratio μ of mass ejected from laboratory craters and secondary craters of Copernicus to the mass of projectiles that produced the craters; μ is plotted vs the range, R_S, that the projectiles or primary crater ejecta would have travelled on the Moon. Two different impact angles are indicated. Horizontal brackets indicate width of annular rings containing measured secondary craters (number of which is indicated). The vertical brackets give the range of values of μ for secondary craters measured within an annular ring.

determine the mass ejected from a secondary crater relative to that of the impacting fragment, further experiments were conducted wherein lexan projectiles were fired into quartz-sand targets at impact angles (measured from the normal) of 60° and 75°. Two orthogonal profiles of each crater permitted a calculation of crater volume and, therefore, ejected mass. Using the studies of Johnson *et al.* (1969) and assuming a spherical-segment geometry and depth-to-diameter ratio of $\frac{1}{4}$, one can show for constant projectile kinetic energy and impact angles that the ejected mass for a crater on the Moon is 1.89 times that on Earth. Thus, this conversion factor was applied to each experimental value of ejected mass to yield a corresponding lunar value. The ratio, μ, of the lunar ejected mass to projectile mass is plotted in Figure 6 as a function of range, R_S, calculated from the impact velocity and angle by using Equation (2) of Oberbeck and Morrison (1974). The figure shows that the data for each impact angle can be described by an empirical equation of the form

$$\mu = KR_S^a, \tag{1}$$

where K and a are constants. For both impact angles the value of a is $\frac{1}{3}$, and the values of K are 107.0 and 73.0 for 60° and 75°, respectively. The data show that if lunar secondary craters are similar in size to laboratory craters, then for ranges as small as 50 km, well-developed craters are produced because μ is greater than 200. Extrapolation of the 75° data shows that local mass ejected and deposited by laboratory-size secondary craters at ranges from 50 km to 2000 km varies from 270 to 920 times the primary-crater ejecta mass. These values compare favorably with values ranging from 1340 to 2034 calculated for the small artificial lunar impact craters produced by Rangers 7, 8, and 9. The Ranger values, derived from data of Whitaker (1972), are slightly higher than the laboratory results because of correspondingly higher impact velocities. These results are compatible with earlier conclusions that ray material of large craters is not mostly primary-crater ejecta but must be mostly locally derived (Oberbeck, 1971a).

Values of mass ratios calculated from Equation (1) are valid only for laboratory-size secondary craters (10–20 cm in diam formed in noncohesive quartz sand). Scaling law considerations based on explosion craters that simulate impact crater formation show that μ also is a function of crater size (for details see Appendix A)

$$\mu = 46.4\left[\frac{\sin 2\theta_S}{2\tan(R_S/3472)} + \sin^2\theta_S\right]^{-1} D_{rs}^{-0.401}\cos^{1.134}\theta_S, \tag{2}$$

where θ_S is impact angle measured from the surface normal and D_{r_s} is the secondary-crater rim diameter in kilometers.

By using this equation, values of μ were estimated for the larger secondary craters of Copernicus from measurements of their rim diameters and range from Copernicus. Crater diameters were measured for craters at radial distances of 84 km to 680 km from the center of Copernicus; their rim diameters varied from a maximum of 5.70 km at radial distance of 142 km to 0.32 km at radial distance of 280 km. In the above equation, θ_S was taken to be equal to 75°, which is consistent with the results of

Shoemaker (1962) and Oberbeck and Morrison (1974). To minimize errors in estimating the values of μ, all fragments that produced the secondary craters were considered to have originated from the primary crater at a radial distance of $\frac{1}{2}$ the present primary-crater rim radius, because the launch point of the fragment that produced any given secondary crater is unknown. The averages of values of μ for secondary craters measured within selected annular rings around Copernicus are also plotted in Figure 6 as a function of range. These average values can be described by Equation (1), where $K=0.0183$ and $a=0.87$. This relationship is considered to be approximate for other large primary craters.

2.2.2. *Ratio m_{SC}/m_{PT} of Cumulative Mass Ejected by Secondary Craters to Total Primary Crater Mass*

2.2.2.1. *Derivation.* To derive an equation for calculating for each size primary crater the cumulative mass ejected by all secondary craters, one first obtains an expression for the differential mass dm_S ejected by secondary craters at radial distance R from the center of the primary crater. This is obtained by multiplying the expression of Equation (1) by the differential mass dm_P ejected by the primary crater and thrown to this distance – i.e.,

$$dm_S = \mu\, dm_P = KR_S^a\, dm_P . \tag{3}$$

An expression for dm_P is obtained by assuming that the areal density, δ, of the primary-crater ejecta that impacted the lunar surface varies with distance R according to the following equation

$$\delta = CR^{-b}, \tag{4}$$

where C and b are constants. This equation is that given in Carlson and Roberts (1963) for the ejecta-mass distribution around terrestrial explosion craters. The differential primary-crater-ejecta mass is, therefore,

$$dm_P = 2\pi\delta R\, dR, \tag{5}$$

which becomes, upon substitution of Equation (4),

$$dm_P = 2\pi CR^{1-b}\, dR . \tag{6}$$

Substitution of Equation (6) into Equation (3) yields

$$dm_S = 2\pi KCR_S^a R^{1-b}\, dR . \tag{7}$$

If R_E is the radial distance at which material was ejected from the primary crater, then

$$R_S = R - R_E . \tag{8}$$

Therefore,

$$dm_S = 2\pi KC(R - R_E)^a\, R^{1-b}\, dR . \tag{9}$$

Integrating Equation (9) one obtains for the cumulative mass ejected from secondary

craters at radial distances greater than or equal to R the equation

$$m_{SC} = 2\pi KC \int_{R}^{R_{\max}} (R - R_E)^a R^{1-b}\, dR, \tag{10}$$

where $R_{\max}$ is the maximum observed radial distance to which primary-crater ejecta is thrown.

The total mass of primary-crater ejecta that impacted the lunar surface is obtained by integrating Equation (6) as

$$m_{PT} = 2\pi C \int_{R_0}^{R_{\max}} R^{1-b}\, dR, \tag{11}$$

where R_0 (hereafter called transient-crater radius) is the radius of the crater prior to slumping, if any. It is also equal to the final crater rim radius R_r if no slumping occurs. Upon integration, Equation (11) becomes

$$m_{PT} = 2\pi C(1/R_0^{b-2} - 1/R_{\max}^{b-2})/(b-2). \tag{12}$$

Dividing Equation (10) by Equation (12) gives the following equation for calculating the ratio of cumulative mass ejected from the secondary craters to total primary-crater ejecta mass

$$m_{SC}/m_{PT} = [K(b-2)/(1/R_0^{b-2} - 1/R_{\max}^{b-2})] \int_{R}^{R_{\max}} (1 - R_E/R)^a R^{1+a-b}\, dR. \tag{13}$$

Because the launch point of the fragment that produced any given secondary crater is unknown, the approximation that $R_E = R_0/2$ was used, which, as will be shown, leads to only small variations in the calculated values of m_{SC}/m_{PT}. Substituting this equation into Equation (13) and evaluating the integral in terms of a binomial series, one obtains to a good approximation that

$$\begin{aligned} m_{SC}/m_{PT} = {} & K(b-2)\, R_0^a \{[(R_0/R)^{b-a-2} - (R_0/R_{\max})^{b-a-2}]/(b-a-2) \\ & - a[(R_0/R)^{b-a-1} - (R_0/R_{\max})^{b-a-1}]/[2(b-a-1)] \\ & - a(1-a)[(R_0/R)^{b-a} - (R_0/R_{\max})^{b-a}]/[8(b-a)] \\ & - a(1-a)(2-a)[(R_0/R)^{b-a+1} - (R_0/R_{\max})^{b-a+1}]/ \\ & [48(b-a+1)]\}/[1 - (R_0/R_{\max})^{b-2}]. \end{aligned} \tag{14}$$

By using Equation (14), both maximum and minimum values of the ratio m_{SC}/m_{PT} were calculated for each of two different assumed cases: (1) where crater slumping does not occur and (2) where it does. The values were calculated for primary-crater radii ranging from 25 km to 500 km for the no-slumping case, but from 25 km to only 250 km for the slumping case. In addition, values were calculated for the Imbrium basin, taking the crater-rim radius to be 670 km, the radius of the outer ring according to Hartmann and Wood (1971).

2.2.2.2. *Maximum values of the ratio m_{SC}/m_{PT}.* Maximum values of the ratio m_{SC}/m_{PT} were calculated by assuming that all lunar secondary craters are equal in size to laboratory craters. Such an assumption is unrealistic but it serves to define gross upper limits of the mass ejected by secondary cratering because μ varies inversely with crater diameter, D_r, (see Equation (2)) and because most lunar secondary craters are larger than laboratory craters. Furthermore, it was assumed again that the ejection angle and, therefore, impact angle is 75°, and that the extrapolation of Figure 6 applies. Thus, Equation (14) was used with values of 73.0 and $\frac{1}{3}$ for K and a, respectively. Although values for b from 3.7 to 4.5 have been reported (Carlson and Roberts, 1963; and Marcus, 1968) for Teapot Ess, a terrestrial explosion crater with a shallow depth of burst which has been used previously as a model for impact crater events (Shoemaker, 1963), a value of 3 was used in the above calculations to compensate for the lack of atmospheric drag and the lower gravity of the Moon. This value agrees with that used in the calculations by McGetchin *et al.* (1973). The upper limit of integration, R_{max}, was assumed in each case to be equal to twelve times the crater rim radius, a limit observed by Baldwin (1963) of the extent of ray patterns around various sized lunar craters. For each primary crater size the maximum values of the ratio m_{SC}/m_{PT} were calculated only for radii greater than the observed radial limit of the continuous deposits, as given in Figure 3.

To calculate the values for the nonslumping case, the transient crater radius, R_0,

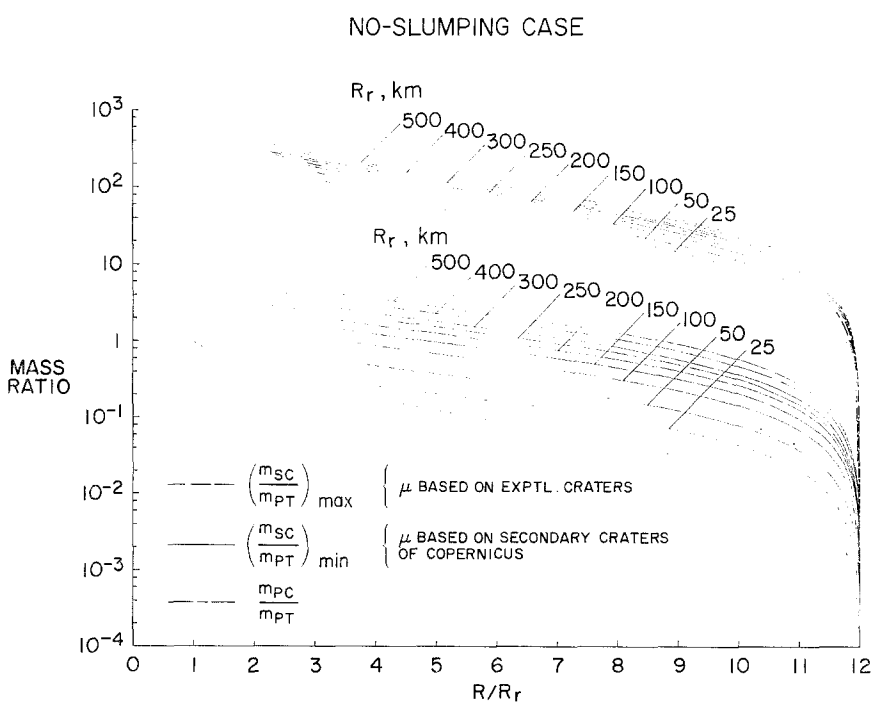

Fig. 7a.

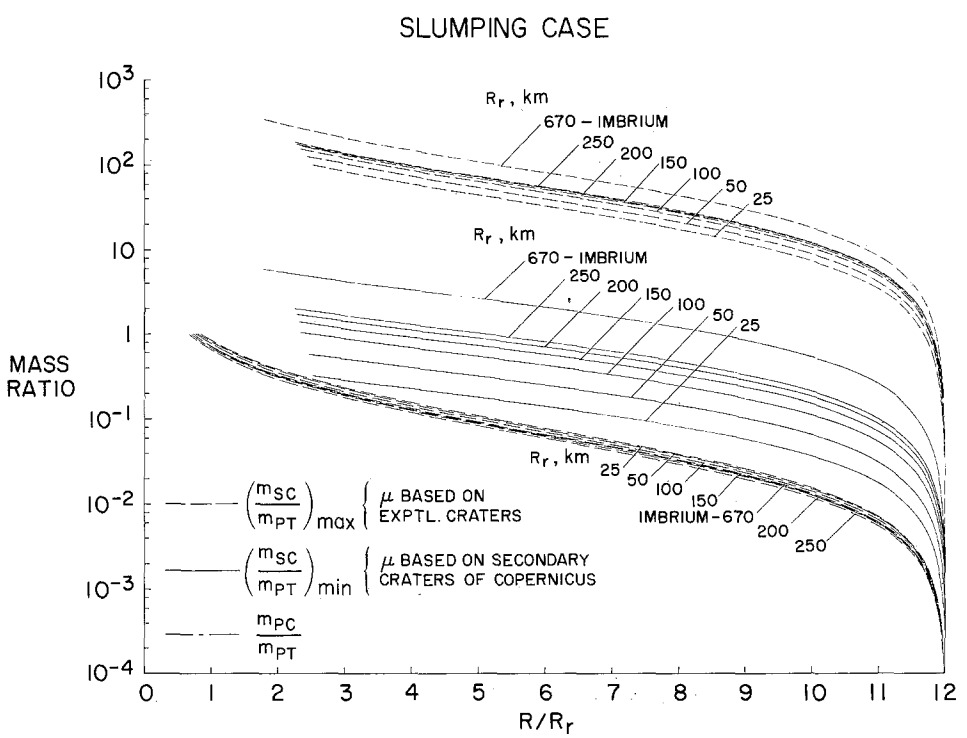

Fig. 7b.

Fig. 7. Maximum and minimum values of the ratio of cumulative mass, m_{SC}, ejected by secondary craters at radial distances greater than R to total primary crater ejecta mass, m_{PT}; and values of the ratio of cumulative mass, m_{PC} of primary ejecta that impacted the lunar surface at radial distances greater than R to total primary crater ejecta mass, m_{PT}. These ratios are plotted vs the ratio of radial distance R to transient crater radius, R_0 and are shown for various size primary craters for each of two different cases: (a) if crater slumping did not occur and (b) if it did.

in Equation (14) was taken to be equal to the crater rim radius, R_r. For the slumping case, however, the transient crater radius was determined from the present crater rim radius, for craters ranging in size up to 250 km in radius, by using estimates for crater slumping given by Short and Forman (1972). Except for the Imbrium Basin maximum values for the ratio m_{SC}/m_{PT} for craters larger than 250 km radius were not calculated because estimates given for slumping of craters this large vary considerably (Short and Forman, 1972; Hartmann and Wood, 1971; Dence *et al.*, 1974). For Imbrium, the transient crater radius was assumed to be 485 km, the radius given for the central ring by Hartmann and Wood (1971). This assumption is in accordance with Head's (1973) interpretation of the Orientale basin: the central ring (the outer Rook Mountains) represents the rim of the final crater cavity prior to slumping.

The maximum values of the ratio m_{SC}/m_{PT} are given for the no-slumping and slumping cases in Figures 7a and b, respectively, vs the ratio of radial distance, R, to crater rim radius, R_r. For comparison, corresponding values are plotted for the ratio of the

cumulative mass, m_{PC}, of primary-crater ejecta that impacted the lunar surface at radial distances equal to or greater than R to the total primary-crater-ejecta mass, m_{PT}. This ratio was calculated by using the values stated previously for b, $R_{\max}$, and R_0 in the equation

$$m_{PC}/m_{PT} = [(R_{\max}/R)^{b-2} - 1]/[(R_{\max}/R_0)^{b-2} - 1], \tag{15}$$

which can be derived by integrating Equation (6) between the limits of R and $R_{\max}$ and dividing the resultant equation by Equation (12).

Figures 7a and b show for primary craters ranging in size from 25 km to 250 km in radius, that the maximum values of the total mass ejected by all secondary craters in the satellitic crater field vary from 118 to 284 times the total primary-crater-ejecta mass if no crater slumping occurred, and from 100 to 184 times if it did. In addition, the figures show that beyond any given radius, the maximum value of the cumulative mass ejected by secondary craters exceeds the cumulative mass deposited by the primary crater by more than two orders of magnitude, which compares with the values of μ given in Figure 6. Although the maximum values for the ratio m_{SC}/m_{PT} are probably not realistic for lunar cratering the values represent theoretical upper boundaries. Their approximate orders of magnitude can be obtained simply by assuming that the ratio μ is constant with R and equal only to 250, a value less than any experimental value given in Figure 6 and by multiplying this value times the values of the ratio m_{PC}/m_{PT} at corresponding radii. In addition, the assumption that all material was ejected from a radial position of $R_E = R_0/2$ was tested by variation of this launch point from the crater center to the crater rim, which showed that values of m_{SC}/m_{PT} varied by only $\pm 4\%$.

2.2.2.3. *Minimum values of the ratio* m_{SC}/m_{PT}. The minimum values of the ratio m_{SC}/m_{PT} were calculated by using Equation (14), in a similar manner as for the maximum values, except that values of 0.0183 and 0.87 were used for K and a, respectively. The values of K and a correspond to estimated values of μ, from Figure 6, based on measurements of the larger secondary craters of Copernicus. Minima result because the values of K and a, determined by using only the larger secondary craters, lead to underestimates of the values of μ (see Equation (2)).

The minimum values of the ratio m_{SC}/m_{PT} are also plotted in Figures 7a and b. They are strictly valid only for a 50-km-radius crater because measurements of μ were made only for secondary craters of Copernicus. Minimum values for other primary crater sizes are less certain because the size of their secondary craters and, thus, their values of μ are different. Although more precise minimum values cannot yet be computed for other primary-crater sizes, the results of Figure 7 are approximately those expected. If secondary craters of other primary craters are as large as those of Copernicus, then for primary craters ranging in size from 25 km to 250 km in radius the minimum values for total mass ejected and deposited locally by secondary craters in the satellitic crater field varies from about 0.37 to 2.9 times the total primary-crater-ejecta mass if crater slumping has not occurred and from 0.32 to 2.0 if it has.

2.2.3. *Conservation-of-Energy Considerations*

According to Figures 7a and b the mass excavated by secondary craters can exceed that of the primary crater. This may seem unfeasible because the total kinetic energy of the primary ejecta is less than that of the impacting meteorite. This, however, is possible because an ejecta fragment is more efficient than the much larger meteoroid in excavating a given amount of crater mass per unit kinetic energy because the meteoroid's much higher impact velocity produces more waste heating than the ejecta fragment on impact. Although the kinetic energy of all the primary-crater ejecta that impacts beyond the continuous deposits does not exceed 38% that of the original meteorite – even for primary craters ranging in size up to 250 km radius – the cratering efficiency of a small secondary crater (0.3 m in diam) may be more than 48 times that of a large primary crater (80 km in diam) (see Appendices B and C). Therefore, the law of conservation of energy is not violated by the above calculations.

2.2.4. *Application of Calculated Results*

As an example of applying the results of Figure 7, the relative cumulative mass ejected by secondary craters of the Imbrium impact at $R \geqslant 1700$ km, i.e., at and beyond the Apollo 16 landing site, may be determined. Since $R_r = 670$ km, the ratio $R/R_r = 2.54$. For such a ratio one finds that secondary craters of Imbrium have ejected locally derived masses 4.8 to 250 times larger than the total basin ejecta delivered to these sites. The correct value depends on the actual size frequency distribution of the secondary crater population. The actual masses are believed to be near the minimum value because most of the secondary craters observed around Imbrium, like those of Copernicus, are orders of magnitude larger than laboratory craters.

2.3. Implications for the Origin of the Smooth-Plains Formation

Simulations, observations and calculations presented above show conclusively that the Cayley formation and other smooth plains can neither exclusively nor mainly consist of ejecta from distant basins. Such ejecta, upon impact with rugged highland terrain, would have produced numerous secondary craters and thus generated large amounts of mass-wasted debris. However, significant deposits of local primary crater ejecta from nearby highland craters need also to be considered (Head, 1974).

Simulated and derived values of μ, i.e., the mass ratio of locally derived materials to that of the primary ejecta, represent useful indices of the amount of primary crater ejecta in the deposits of secondary craters. However, the final proportions are determined by these values only in part, because they depend also on the degree to which later arriving materials rework the deposits produced by earlier secondary craters. However, such reworking would occur to a significant degree only under highly idealized circumstances which in reality do not exist for impact in the lunar highlands. For example, consider the hypothetical case of a large primary crater that forms in a perfectly smooth level plain and that ejects only small fragments comparable to those used in the laboratory simulation. Each of these upon impact produces a laboratory-

size secondary crater and they would, acting together, produce a saturated zone of secondary craters in the surrounding area. Although Figure 7 predicts that these craters eject quantities of material that represent many multiples of primary-crater mass, they would do so by re-excavating material ejected and deposited by earlier-formed secondaries. This conclusion follows from the fact that the thicknesses of deposits surrounding the primary predicted from the total calculated mass ejected by small secondaries greatly exceeds the secondary crater depth. Therefore, the deposits emplaced by the secondary craters are mostly primary-crater ejecta. On the other hand, if the primary crater forms in rugged terrain, large amounts of reworking does not occur since the earlier-formed secondary craters eject material downhill and produce slides, thus exposing new material to impact. The small secondary craters formed by later arriving fragments eject new material each time and in this case form local deposits in depressions consisting mostly of thick deposits of mass-wasted local debris. Therefore, reworking to a significant degree can occur only for the ideal case of impact in a target consisting of only small particles in a perfectly smooth level plain, a case that does not exist on the highlands and probably does not exist anywhere on the Moon. Moreover, each ejecta fragment can produce a secondary crater only if the time between impacts of the fragments is sufficient to allow for deposition of all secondary crater ejecta before the impact of later-arriving ejecta. In fact, this impact sequence is not realistic. Gault *et al.* (1968) and Oberbeck and Morrison (1974) have observed that impact of ejecta of laboratory and lunar craters, respectively, proceeds from the crater rim outwards. That is, material impacts at a given range only at one given time. Such conclusions are further supported by results suggesting that material transported beyond the continuous deposits is ejected in a very restricted range of angles (Shoemaker, 1962; and Oberbeck and Morrison, 1974). Ejecta fragments impacting at a given range all have about the same velocity, and the flight time for each fragment is about the same. Therefore, the time between impacts of two adjacent fragments is probably insufficient to permit deposition of ejecta of the secondary crater produced by the first fragment before the second fragment impacts. In fact, such short times between impacts for small fragments impacting at nearly the same range would cause the fragments to act as a much larger single projectile which would produce a large secondary crater, in agreement with the distribution of large secondary craters observed on lunar photographs.

In reality most secondary craters of large primary craters are probably not laboratory size or smaller but are similar to those observed in lunar photographs. If, instead, they were very small, many primary craters in the highlands would not be visible because of the huge masswasted deposits as predicted by Figure 7. With the assumption that most secondary craters of large primary craters are the size of those observed on high resolution lunar photographs, then according to Figure 7 all secondary craters eject from only 0.32 to 2.9 times the primary crater-ejecta mass, depending on whether or not crater slumping is assumed. One can show that even if all this material were spread uniformly around the primary crater, then the thickness of such a deposit would be small compared to the depths of the secondary craters. Thus, little reworking

within the primary ejecta would occur and the secondary craters would eject predominantly local material. In addition, since the secondary craters and clusters are well separated, the deposits of secondary craters should be on the average well separated and little if any reworking of the primary ejecta can occur. Material has probably not impacted at the site of previously impacting debris. Thus, the values of μ calculated with Equation (2) and plotted in Figure 6 represent lower bounds on the ratios of local material deposited by observed secondaries and material deposited by primary craters.

The implications regarding the origins of the smooth plains are that (1) large mass-wasting deposits should form between and inside large lunar craters if there is a high primary-crater density and (2) those parts of the plains deposits produced by a given primary crater consist largely of that crater's ejecta only if the crater is nearby. For example, data of Figure 6 show that μ is less than 1 (primary ejecta $> 50\%$ of combined primary-and-secondary-ejecta deposits) only for ranges less than 100 km from the points within the primary crater at which ejecta was launched. Thus, those parts of a smooth plains formation produced by a given primary crater consist mostly of primary-crater ejecta only if the formation is within 100 km of these launch points. Conversely, they consist mostly of local material if the formation is far from the primary crater. For a source crater at a distance of 1000 km, μ is 7.4, according to Figure 6, and therefore 12% of the combined primary-and-secondary-ejecta deposit consists of primary-ejecta material. Since both Imbrium and Orientale are at distances greater than 1000 km from the Apollo 16 site, the materials returned from that site cannot be mainly Imbrium or Orientale ejecta or mainly ejecta of any other distant crater. Material emplaced by a distant crater is mostly material mass wasted from the surrounding highland topography by secondary craters. However, material emplaced in smooth plains by nearby craters is largely primary crater ejecta with smaller amounts of mass-wasted material.

In summary, the cratering mechanics calculations predict that material thrown from a lunar crater of 100-km radius or larger produces secondary craters that eject and deposit masses of local material exceeding that ejected from the primary crater. Moreover, the calculations predict significant mass-wasted deposits in the smooth plains of the lunar highlands that should show evidence of secondary cratering. The following section demonstrates that secondary craters are present in the Cayley Formation and other smooth plains areas.

3. Secondary Craters on the Cayley Formation and Other Smooth Plains

Ptolemaeus crater is an example of a large depression containing Cayley Formation (Figures 1 and 8). Many crater chains and clusters occur in this area. A very long crater chain crosses from the highlands onto the floor of Ptolemaeus and extends into Alphonsus crater (Figure 8a). Ridges (indicated by arrows) associated with this subdued chain support the hypothesis that it is a huge secondary-crater chain (Oberbeck and Morrison, 1974). The secondaries are well defined on the floors of Ptolemaeus and

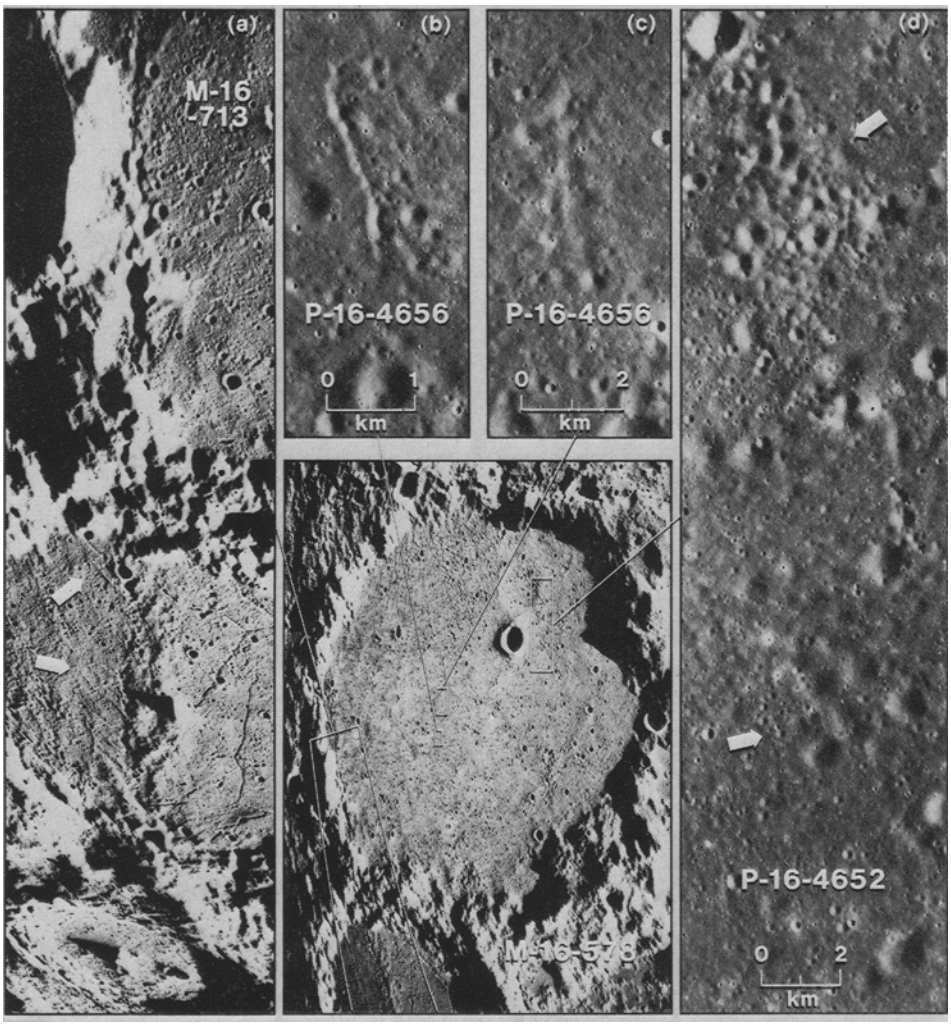

Fig. 8a–d. Secondary crater chains and clusters in the Cayley Formation on the floor of Ptolemaeus Crater. (a) Parts of lunar craters Ptolemaeus and Alphonsus and large secondary-crater chain with associated *V*-shaped ridges (indicated by arrows). (b) Secondary-crater chain older and more subdued than chain shown in Figure 8a. (c) Secondary-crater chain older than chain shown in Figure 8b. (d) Secondary-crater clusters (indicated by arrows) in two different stages of preservation.

Alphonsus, but where they cross the highlands between these two craters they are not. This secondary-crater chain is viewed as the most recent one of its size that has eroded material from the highlands and rim of Ptolemaeus and that could have deposited material over a large area of the floor of Ptolemaeus, thereby adding material to the Cayley Formation. Numerous other crater chains and clusters also occur on the floor of Ptolemaeus. For example, Figure 8b shows a crater chain that is older than the one shown in Figure 8a but younger than the very subdued crater chain shown in Figure 8c.

Figure 8d shows a large, fresh crater cluster and also a small cluster of very subdued craters. Thus, many large highland craters, intermediate in age between the ancient crater Ptolemaeus and the unidentified younger crater that produced the very fresh secondary-crater chain (Figure 8a), must have produced countless secondary-crater chains and clusters on the highlands and on the crater floor.

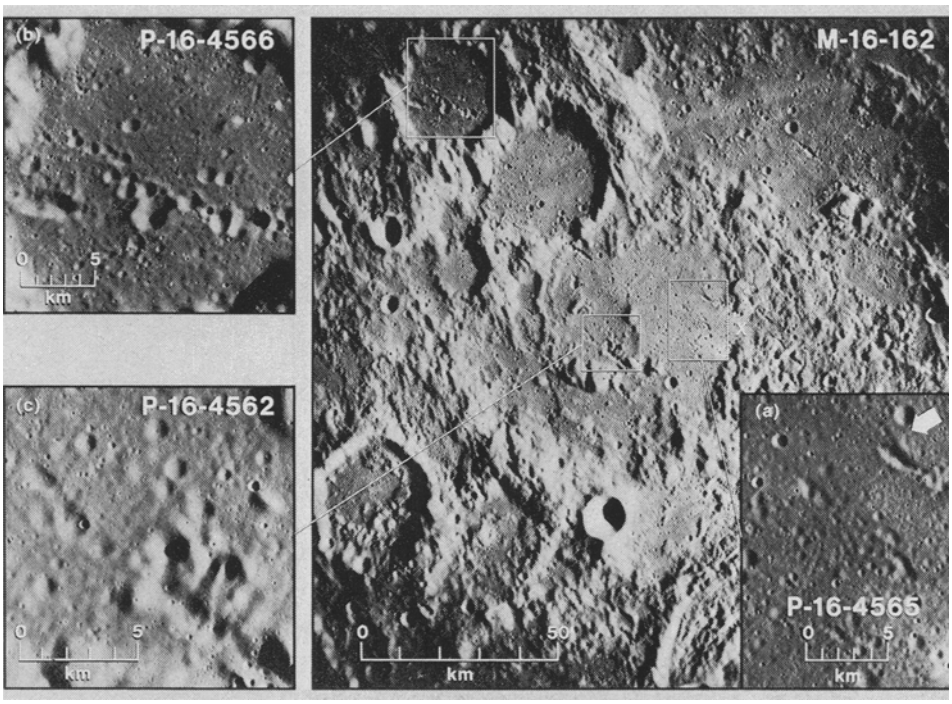

Fig. 9a–c. Cayley Formation near the Apollo 16 landing site (marked as X). (a) Relatively fresh secondary-crater chain (indicated by arrow) of Theophilus Crater with V-shaped ridges and very subdued cluster of secondary craters. (b) Large secondary-crater chain in Dollond C Crater. (c) More subdued and older secondary-crater chain.

Numerous secondary craters are present also near the Apollo 16 landing site. One example is the fresh crater chain of Figure 9a, which has a herringbone ridge component, indicating an origin by secondary impact (Oberbeck and Morrison, 1974). More eroded chains and clusters are also visible. Another example is a very large fresh, subdued crater chain in the crater Dollond C, shown in Figure 9b. Figure 9c shows an even more subdued crater chain. Members within any given chain or cluster typically display the same state of preservation that is diagnostically different from members of other chains or clusters, reflecting simultaneous formation for any given cluster or chain.

Figure 10 shows a photograph of the Davy crater chain which occurs partially in the Cayley Formation on the floor of Davy Y crater and partly on the crater's rim and

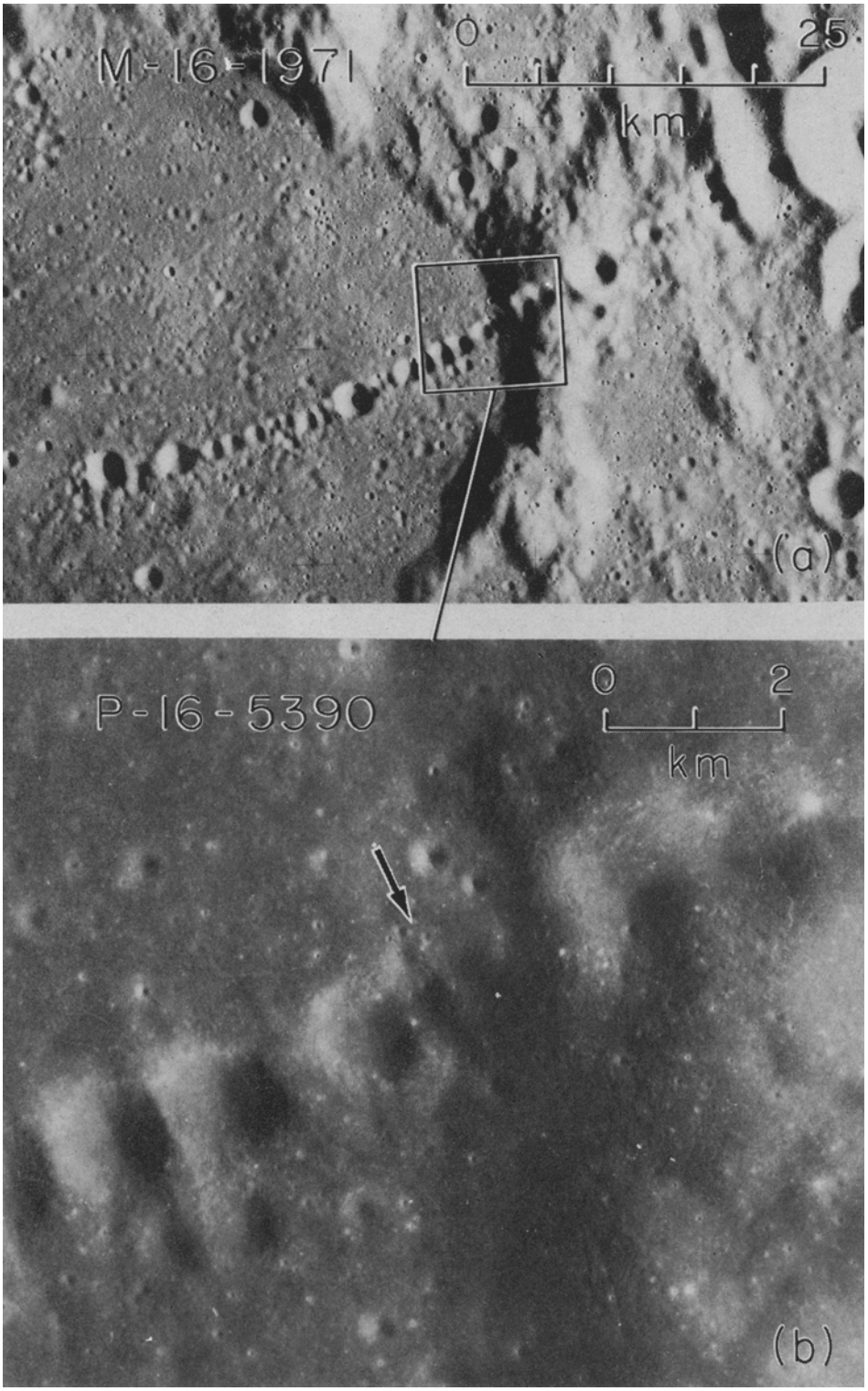

Fig. 10a–b. (a) Davy Crater chain crossing from floor of Davy Y crater into highland terrain. (b) Magnification of area outlined in Figure 10a, showing partially filled craters.

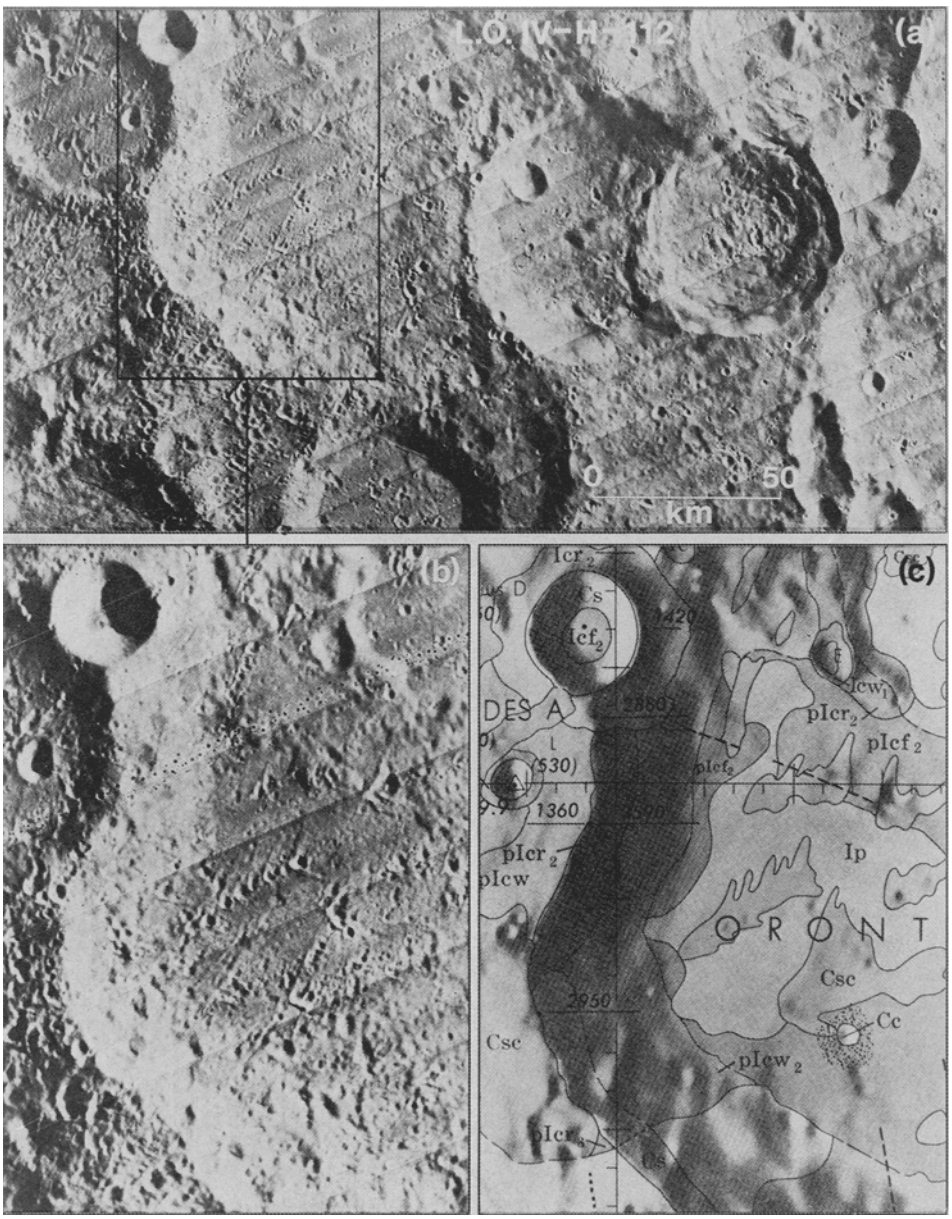

Fig. 11a–c. (a) Area east of Tycho crater. (b) Magnification of area outlined in Figure 11a, showing mass wasting of ridge by secondary craters of Tycho and smooth plains area to the East. (c) Portion of geologic map by Pohn (1972) showing areas of Figure 11b mapped as smooth plains (Ip) and as secondary craters (Csc).

the adjacent highland. Until recently this crater chain was thought to be of volcanic origin (Mutch, 1972), like the Cayley Formation. However, study of Apollo 16 high resolution panoramic photographs revealed the presence of ridges that radiate from intersections of craters in the chain (Figure 10a), indicating that it is a secondary-crater chain (Oberbeck and Morrison, 1973). Figure 10b shows the area at the base of the Davy Y crater wall. Stereoscopic observations show that craters nearest the wall have been filled (arrow), as a result of mass wasting triggered by secondary-impact cratering.

Figure 11a shows the area just east of Tycho crater. Smooth plains are shown enlarged in Figure 11b and mapped (I_p) in Figure 11c. These plains, like Cayley plains in every way, obviously have been profoundly influenced by secondaries of Tycho. These secondaries must have deposited large amounts of highland material on to the smooth plains at lower elevations. These plains are only 130 km from Tycho; μ is therefore equal to one (Figure 6). Thus, the secondary craters formed on the highlands just west of the smooth plains ejected material that was approximately one-half highlands material and one-half Tycho ejecta. This implies that large highland craters near areas like the smooth plains in Ptolemaeus could also contribute relatively high proportions of their crater ejecta to the plains units.

Massive secondary cratering can also transport large quantities of local highland material over large lateral distances by formation of highly efficient landslides and thus can produce nearly level plains. Howard (1973) has examined the process of lunar landslide formation and has offered convincing evidence of their high efficiency. Moreover he has illustrated some landslides on the interior walls of craters that were triggered by secondary impacts. The authors also have observed examples of landslides triggered by secondary impacts. Figure 5c shows one example: a landslide triggered by impact of fragments on a ridge. Based on stereoscopic observations, mapped area C defines the thickest part of the landslide. Area D probably contains landslide material also, since a thin deposit appears here and the small craters are much less frequent than on adjacent terrain. At areas A and B are thick deposits that could be either landslide debris or secondary-crater ejecta. The largest lunar landslide discovered to date is shown in Figure 12 (position A). It extends 5 km from the base of the massif. Howard (1973) noted evidence for triggering of this landslide by secondary cratering. The authors also believe it was triggered by impact of the fragments that produced the secondary craters at the top of the massif (position B in Figure 12).

Subdued secondary-crater chains and clusters in the Tycho area, on the Cayley Formation at the Apollo 16 landing site, and on the floors and walls of Ptolemaeus and Davy Y craters and the surrounding highlands indicate that these areas could have received the massive bombardment of simultaneously impacting fragments of primary-crater ejecta predicted by the calculations. The large number of primary highland and maria craters and large multiringed basins surrounding these smooth plains are the apparent sources for these fragments. Secondary craters produced on nearby slopes would have ejected and deposited in the floors of large craters and other depressions material containing proportions of primary-crater ejecta in an amount varying in-

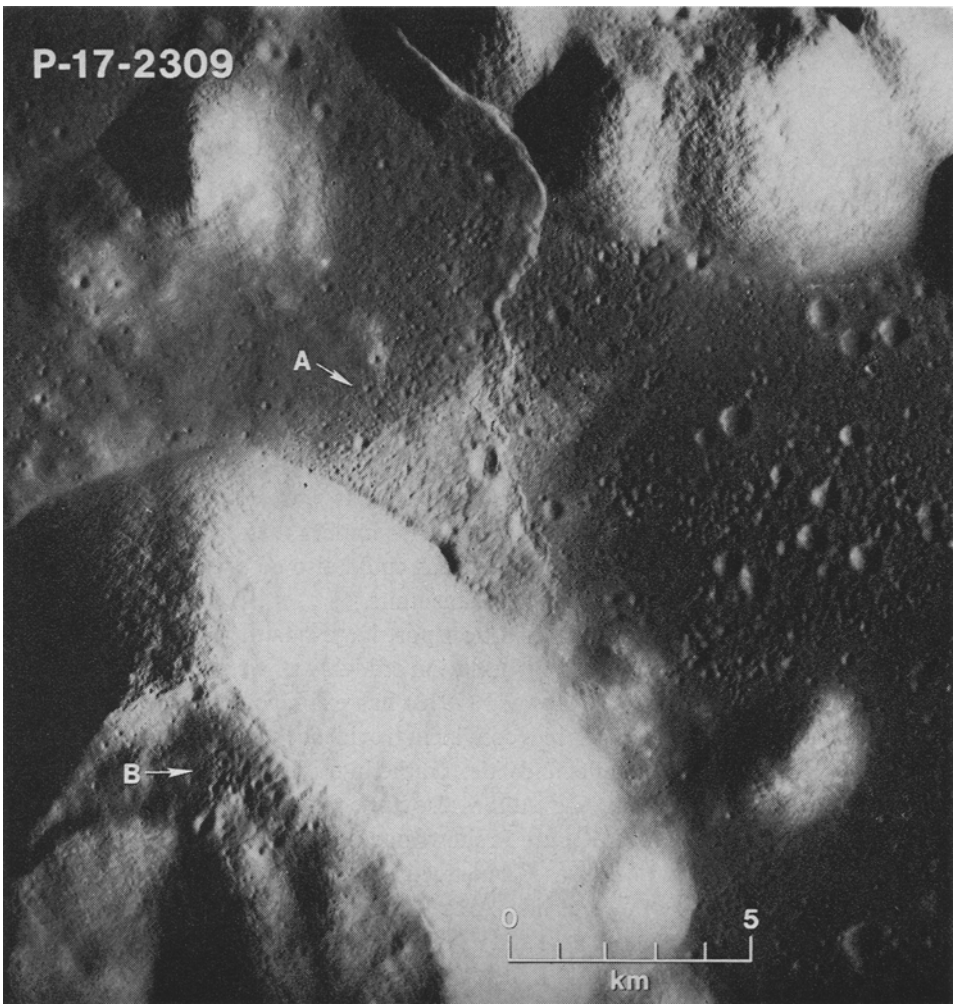

Fig. 12. Lunar surface area near the Apollo 17 landing site and landslide (A) caused by secondary craters (B).

versely with the distance from the source primary crater. Also, nearby highland craters would have added significant amounts of their ejecta to these smooth-plains areas. This addition of material and spreading of the material by subsequent secondary cratering and landslides produced by such cratering could thus lead to gradual buildup of large level plains.

In summary, because of their subdued character, even when fresh, and because of their still poorer development in rugged highland terrain, the influence of secondary craters has been underestimated. The immense volume of material that can potentially be excavated and redistributed by these craters represents a powerful erosional and depositional mechanism that must have contributed significantly to the evolution of

the lunar surface, particularly to the highland terrains having large populations of large primary craters.

If many highland craters are correctly mapped as pre-Imbrian, then secondaries of Imbrium could have contributed to the production of the Cayley Formation on the floors of these craters. However, many highland and mare craters are post-Imbrian and so must also have contributed to its production. Thus, Cayley-type deposits must have been emplaced over a long period of time from pre-Imbrian to post-Imbrian time.

4. Remote Measurement of the Smooth-Plains Formation

A variety of remote measurements of the physical and chemical properties of the smooth-plains materials is consistent with the hypothesis that it was emplaced mainly by relatively small craters such as secondary craters. The albedo measurements of Pohn and Wildey (1970) indicate that the albedo of these plains at different localities is different. Yet the absolute albedo of an individual occurrence has strong affinities to the surrounding highlands terrain.

Telescopic spectral-reflectivity work in the wavelengths 0.3 to 1.1 μm (Adams and McCord, 1972; McCord *et al.*, 1972a, b) show that lunar highland materials are diagnostically different from mare surface. Within highland areas, however, differences are subtle, if present at all. Observed differences are best explained by various ratios of glass to crystalline materials thought to reflect an aging effect due to continuous meteoroid bombardment. The smooth-plains formations do not possess diagnostic spectral characteristics; on a local scale they seem indistinguishable from their surroundings.

Geochemical investigations along the lunar ground tracks of the Apollo 15 and 16 Command Modules may provide significant data for interpretation of the nature of the formations. The gamma-ray-spectrometer results (Trombka *et al.*, 1973) and those of the X-ray spectrometer (Adler *et al.*, 1973) are illustrated in Figures 13 and 14, respectively. The fractional surface area per resolution cell covered by smooth-plains formation was determined for the above experiments by planimetric measurements of the geological map by Wilhelms and McCauley (1971). Figure 13 shows that separated resolution cells with equal areas of plains materials often exhibit different gamma-ray counts, but adjacent resolution cells with different proportions of plains often exhibit similar gamma-ray counts. For example, the area from 8°S to 12°S lat. and from 16°W to 12°W long. is characterized by equivalent gamma-ray activity, but the percentage of plains in each of the 4 resolution cells varies from 10 to 70%, and a cell with as little as 10% plains is adjacent to a cell with as much as 70% plains. The data of Figure 14 show examples of adjacent surface areas with very different percentages of plains formation but nearly equal Al/Si and Mg/Si ratios. Although Figure 14 does not show it, Adler's tabulated results (Adler *et al.*, 1973) show similar Al/Si and Mg/Si ratios for the center of Ptolemaeus crater and for the highlands east and west of Ptolemaeus. The data obtained while flying over the mapped smooth-plains localities (see Figures 13 and 14) demonstrate that the chemical makeup of the plains may be

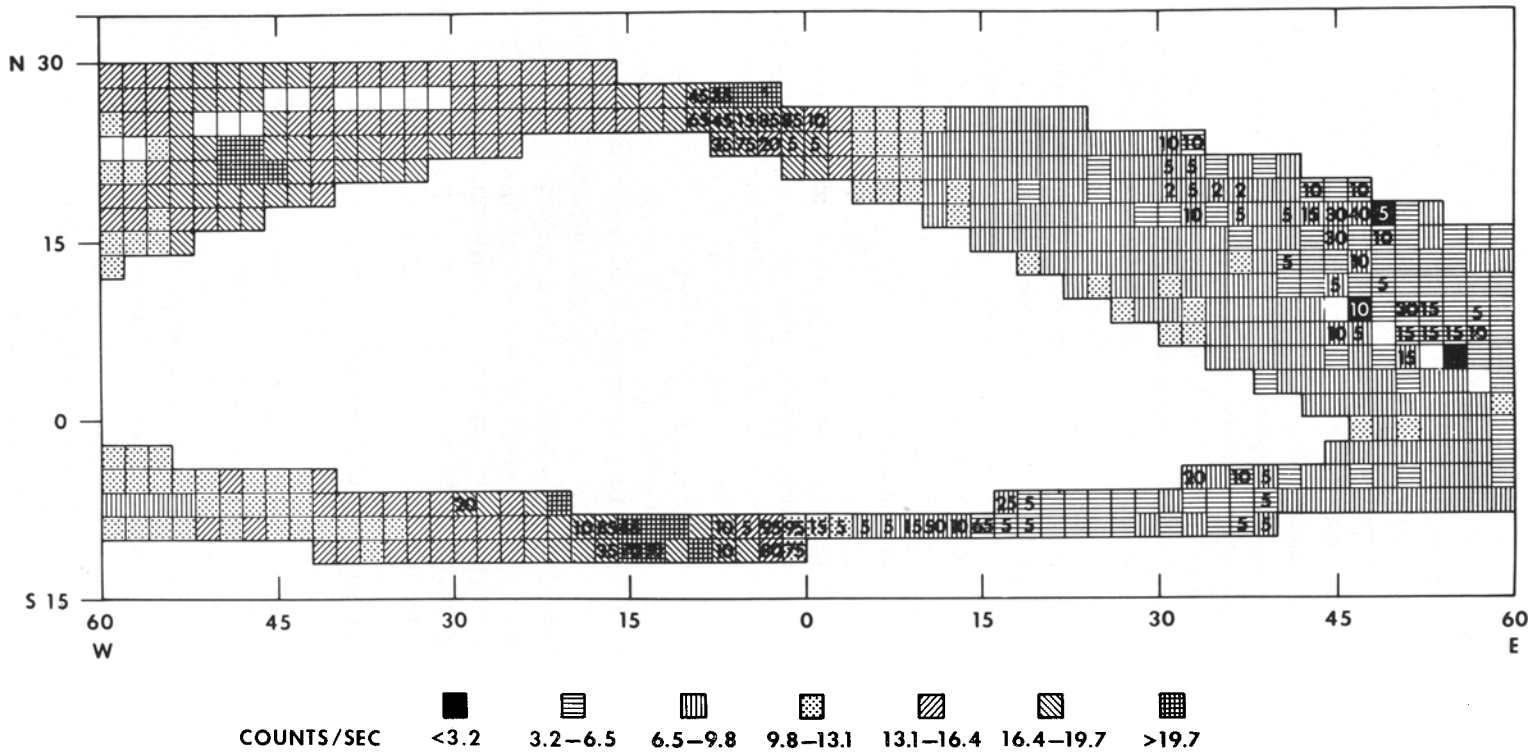

Fig. 13. Distribution and concentration of radioactive elemental species like Th, U, etc., according to Trombka *et al.* (1973). Superimposed numbers are the percent of surface area per resolution cell covered by smooth plains as obtained by planimetry.

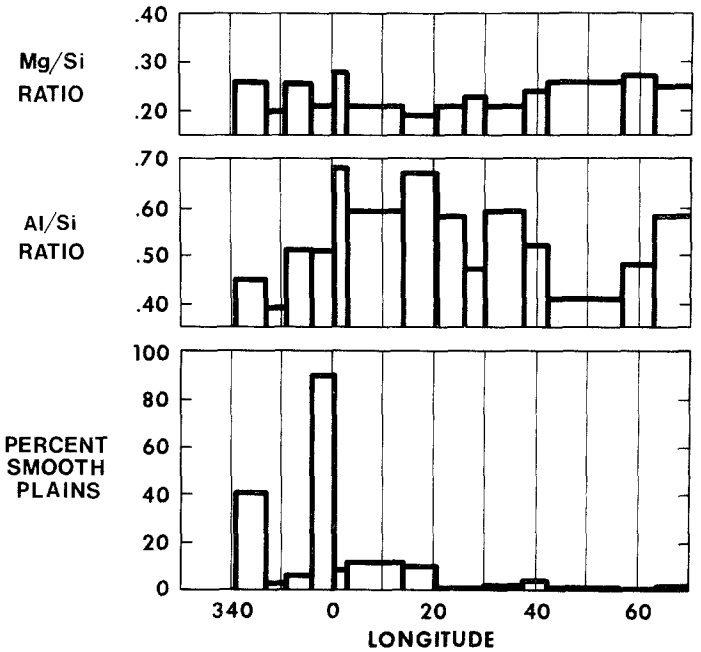

Fig. 14. Mg/Si and Al/Si ratios along the Apollo 16 ground track (Adler *et al.*, 1973) and amount of Cayley plains along the same track.

different from locality to locality and – most importantly – that although one area may differ from another most have close affinities to nearby highland terrain.

Remote-sensing studies reveal that mapped smooth plains have close affinities ot their surrounding terrain. The fact that they blend in with local highland terrain is compatible with the hypothesis that small craters have indeed transported highlands material into depressions and thus produced the plains formations.

5. Discussion

Historically, the Cayley Formation has been associated genetically with formation of the Imbrium Basin because it is peripheral to the Fra Mauro Formation. Published hypotheses for emplacement of the Cayley Formation involve deposition of continuous deposits of ejecta from multiringed basins even though the basins are hundreds of kilometers from the supposed sites of deposition. For example Chao *et al.* (1973) have hypothesized, based on the apparent similar age of the Cayley Formation and the Hevelius Formation as well as petrographic considerations, that material of the Cayley Formation was ejected from Orientale Basin in ballistic trajectories and was deposited as a layer thousands of kilometers away at the Apollo 16 site. Hodges *et al.* (1973) also have hypothesized that the Cayley Formation resulted from material that was ejected from one or more impact basins in ballistic trajectories and deposited hundreds

of km away. These mechanisms, however, are improbable because the supposed sites of deposition are outside the continuous deposits of the basins. Primary ejecta beyond the continuous deposits produce not deposits but isolated craters or crater chains that eject and deposit local material.

Therefore, the contemporaneous emplacement of the smooth plains (Soderblom and Boyce, 1972) and the similarity in age with the Hevelius Formation (Chao *et al.*, 1973), the continuous deposits of Orientale basin, may only be apparent. Some secondary craters resemble eroded primary craters used in the above dating method. Moreover, an area recently exposed to secondary cratering could resemble an area cratered over a long period of time, thus leading to errors in surface dating. Also, a source of error arises in the dating method employed when the ejecta deposits being dated are thin relative to the size of the crater used to date the surface (Soderblom and Lebofsky, 1972). McGetchin *et al.* (1973) have estimated only two meters of Orientale ejecta, at most, in the Apollo 16 site. The large craters (>500 m) used to date such a formation (Chao *et al.*, 1973) must therefore have been formed on a previously produced surface because the craters used in determining its formation age are only slightly altered, if at all, by a 2 m thick deposit. Therefore, inferred age similarities of the Hevelius formation and the smooth plains would require that the surface deposits at the Apollo 16 site are not from Orientale basin.

Emplacement by secondary craters, however, could be the dominant mechanism for origin of the smooth-plains materials. This conclusion rests on the following independent observations and calculations:

(a) Material ejected beyond the continuous deposits of large lunar primary impact craters has produced secondary craters, not deposits of primary crater ejecta. For the craters Kepler, Copernicus, and Aristarchus this cratering regime starts at distances as close as 50 km from the crater rim. Secondary craters typically eject masses of local material equal to multiples of that of the fragments producing the craters.

(b) Calculations indicate that secondary craters in the satellitic cratering field eject a mass of material varying from fractions to multiples of the total primary crater ejecta mass. Thus, ejecta of large craters and basins transported in ballistic trajectories to great distances could not have produced continuous deposits consisting solely of primary-crater ejecta at the Apollo 16 landing site, but instead must have produced large deposits consisting mostly of local material ejected by secondary craters.

(c) Examples of relatively large subdued secondary crater chains observed on the Cayley Formation and other smooth plains have been illustrated in this paper. Their different ages indicate that they represent a powerful erosive mechanism that has acted over a long period of time.

(d) The subdued appearance of craters on the smooth plains can be explained by the fact that simultaneous secondary impact produces craters with such an appearance.

(e) A variety of remote sensing measurements suggests that the Cayley Formation differs in composition from place to place but is like the local surrounding highland terrain. Erosion of highland terrain by small craters would produce these relationships.

Observations (a), (b), (c) and (e) are incompatible with one large scale depositional event but are compatible with a local origin of the smooth-plains formation. Therefore, if the smooth plains are related in origin to large craters and basins, a different origin than those previously hypothesized is indicated. Massive bombardment of the highlands by meteoroids has occurred, and the associated secondary fragments have shed material from the intercrater highland terrain and deposited it into local depressions. While it is postulated that the smooth-plains materials might be primarily erosional products and local primary-crater ejecta, it may be that other impact mechanisms and volcanic processes may have also been responsible for some smooth-plains materials.

An additional current impact hypothesis involves a quasi-fluid ejection regime. To account for the morphologic difference between the thick ejecta of the Fra Mauro Formation and the smooth, level Cayley Formation, Eggleton and Schaber (1972) have hypothesized that the smooth-plains materials were emplaced in a fluid ejection regime originating during the Imbrium Basin formation. Moreover, they believe that the fluidizing medium was vaporized target and projectile material and that the masses mobilized were deposited after the thick bulk ejecta. The details of this postulated mechanism have not as yet been published.

A recent proposal by Head (1974) merits special consideration. He proposed that the flat terrain of the Cayley Formation in the Apollo 16 site may reflect in part the original flat floors of ancient craters and that the Cayley materials are fallback breccias and ejecta from nearby craters. The results are consistent with those presented here with regard to the source of the material of the Cayley Formation except that our results imply that large amounts of local primary-crater material and ejecta must have been eroded by secondary craters and small primary craters because very degraded craters were considered by Head as the source of the smooth-plains material. In addition, the cratering theory presented here predicts that small but significant amounts of ejecta of distant primary craters have been deposited in the smooth-plains materials along with the erosional products of their impact.

While secondary cratering is important for emplacement of the smooth plains in their present positions, primary craters probably have produced the textures exhibited by the samples. The severe thermal effects observed in the Apollo 16 breccias could all have been produced by primary meteorite impact; calculations based on equation of state work by Ahrens *et al.* (1973) and others show that the observed thermal metamorphism could not have been produced by isolated individual secondary impacts because the impact velocities are not sufficiently high to produce the shock pressure amplitudes required to cause partial or complete melting. The ubiquity of multiple brecciation of the Apollo 16 samples is strong evidence of formation by multiple events because investigations of terrestrial impact structures and their ejecta deposits (Engelhardt, 1971; Dence, 1971; Kieffer, 1971; and Chao, 1972) as well as small scale crater experiments and consideration of energy partition during the impact process (Gault and Heitowit, 1963) indicate that molten and highly shocked materials make up only a small percentage of the total ejecta mass for a single crater event. Thus, multiple impacts appear to be necessary to account for the petrographic features

exhibited by lunar breccias (see also Dence and Plant, 1972; Short and Forman, 1972).

The results of the cratering theory presented in this paper may also be applied to interpretation of the origin of the material in the continuous deposits surrounding these basins and other large craters. Material in those deposits having no obvious secondary craters has been interpreted as being ejecta from the basins (Eggleton and Schaber, 1972), even at distances that are hundreds of kilometers from the basins and craters. Figure 6 indicates that material thrown this far is capable of excavating great quantities of local material in addition to depositing material from the central crater or basin. Thus, these deposits, consist not only of basin or crater ejecta, as has been traditionally assumed, but also of secondary-crater ejecta. Investigations of the Ries crater, (Hüttner, 1969) show that continuous deposits of the Ries contain large amounts of marley sand mixed with crater ejecta on the periphery of the deposits. This material could not have been ejected from the crater site because the formation was not present within the crater. Instead it must have been mixed with crater ejecta. Thus, considerable care must be used in associating crater continuous deposits with crater ejecta. It now seems certain that the Apollo 14 Fra Mauro samples contain significant amounts of local material in addition to material ejected from Imbrium Basin.

6. Concluding Remarks

When material is ejected beyond the continuous deposits of large lunar craters and basins it produces secondary impact craters when it impacts the lunar surface. Typically, these craters eject masses of local material that exceed the mass of primary ejecta that produces the secondary crater. Therefore, if the lunar smooth plains were emplaced by distant craters and basins it must consist mostly of the ejecta of local primary craters that is emplaced either by secondary craters of distant primaries or directly by local primary craters.

This mode of origin for plains materials is supported by the existence of many secondary crater chains and clusters on the smooth plains surface and by additional calculations that predict large erosional deposits as a result of secondary cratering. Remote measurements of the chemistry of smooth plains materials also support the hypothesis that they are erosional in origin.

Appendix A: Derivation of Equation (2)

Although there are fundamental differences in the mechanics of impact and explosive cratering, explosives detonated at relatively shallow depths of burial appear to provide a reasonable simulation and basis for determining the size and geometry of impact craters. In this manner, by equating explosive energy to the impact kinetic energy, the explosive data may be applied directly to cratering problems for any assumed combination of projectile mass and impact velocity. This procedure has been commonly assumed in the literature (e.g., Baldwin, 1963) and is supported by results from recent small scale laboratory experiments (Oberbeck, 1971b).

Explosive cratering events performed at the Nevada Test Site (NTS) (Teller *et al.*, 1968) suggest that the rim diameter D_r is related to explosive energy E by

$$D_r = kE^{1/3.4}. \tag{A1}$$

To evaluate the constant k for lunar applications, we use the results given in the following table for two shallow-burial, nuclear explosion events: Jangle U and Teapot Ess.

	Scaled depth[a]	Energy (ergs)	D_t(m)
Jangle U	0.13	5.0×10^{19}	80
Teapot Ess	0.5	5.0×10^{19}	89

[a] Scaled depth has customarily been in terms of $h/(W)^{1/3}$, where h is depth of burial in feet and W is the explosive charge weight in pounds TNT equivalent.

As suggested by Baldwin (1963) and Oberbeck (1971b), a scaled depth of 0.25 provides a reasonable approximation for simulating an impact event, and would correspond to a true crater diameter D_t of about 85 m for an equivalent terrestrial impact kinetic energy release of 5.0×10^{19} erg. (True diameter D_t is the crater diameter measured at the original surface.) If the size of craters scale according to Johnson *et al*'s. (1969) results for the effects of differences in gravitational acceleration g, then

$$\frac{D_{t_{\text{Moon}}}}{D_{t_{\text{Earth}}}} = \left(\frac{g_{\text{Earth}}}{g_{\text{Moon}}}\right)^{0.12} = 1.237.$$

But this means $D_{t_{\text{Moon}}}$ would be about 105 m for an impact kinetic energy of $5.0 \times \times 10^{19}$ erg. The relationship between rim diameter D_r and true diameter D_t may be taken for present purposes to be approximately $D_t = 0.85\ D_r$ (Baldwin, 1963; and unpublished small scale impact experimental results), and after substitution in Equation (A1) one obtains for lunar craters that

$$D_r = 2 \times 10^{-7}\ E^{1/3.4}, \tag{A2}$$

where D_r is expressed in kilometers and E is given in erg.

To estimate the mass ejected from a crater of diameter D_r, we assume that a spherical segment represents the crater shape and take the depth to diameter ratio, d/D_t, equal to $\frac{1}{4}$. The mass ejected from a lunar crater, m_e, becomes, therefore,

$$m_e = \pi \varrho_e d[3(D_t/2)^2 + d^2]/6 = 6.52 \times 10^{13}\ \varrho_e D_r^3, \tag{A3}$$

where ϱ_e is the mass density (g cm^{-3}) of the ejected material, m_e is in grams, and D_r is in kilometers. If the geometry of the craters is relatively independent of size,

$$D_r^3 = k^3 E^{3/3.4}.$$

Substituting this into Equation (A3) yields

$$m_e = 5.22 \times 10^{-7}\ \varrho_e E^{0.882}.$$

This relationship is valid, however, only for impacts at normal incidence and a correction must be applied for oblique trajectories. Laboratory experiments (Gault and Wedekind, 1973) indicate for present applications that the mass ejected from a crater varies with $\cos\theta$, so that as a final result one obtains

$$m_e = 5.22 \times 10^{-7}\, \varrho_e E^{0.882} \cos\theta \tag{A4}$$

for relating the ejected mass to the kinetic energy of the impacting particle. Rearranging terms in Equation (A4), substituting Equation (A3), and assuming a value of 3 g cm^{-3} for ϱ_e, we obtain

$$m_e = 3.2 \times 10^{-9}\, E D_r^{-0.401} \cos^{1.134}\theta\,. \tag{A5}$$

Replacing the kinetic energy, E, in Equation (A5) with $mV^2 \times 10^{10}/2$, where m and V are the mass and velocity of the impacting particle, respectively, we obtain for the ratio, μ, of mass ejected from a lunar crater to that of the impacting particle the equation

$$\mu = m_e/m = 16V^2\, D_r^{-0.401} \cos^{1.134}\theta\,. \tag{A6}$$

For secondary craters, we introduce the range equation for ballistic trajectories over a spherical body,

$$V^2 = V_S^2 = R_m g_m \left[\frac{\sin 2\theta_S}{2\tan(R_S/2R_m)} + \sin^2\theta_S\right]^{-1}, \tag{A7}$$

which is obtained by rearranging Equation (2) of Oberbeck and Morrison (1974). Adopting values of 1736 km and 1.67×10^{-3} km s^{-2} for R_m and g_m, respectively, and combining Equations (A6) and (A7), we obtain the following equation for μ for a lunar secondary crater

$$\mu = 46.4\left[\frac{\sin 2\theta_S}{2\tan(R_S/3472)} + \sin^2\theta_S\right]^{-1} D_{rs}^{-0.401} \cos^{1.134}\theta_S\,. \tag{A8}$$

Values of μ calculated from Equation (A8) for various values of R_S, D_{r_s}, and θ_S are given in Table I.

TABLE I

Values of μ calculated from Equation (A8)

Range, R_S (km)	Secondary crater diameter, D_{r_s} (km)	μ		
		$\theta_S = 75°$	$\theta_S = 60°$	$\theta_S = 45°$
50	10^{-2}	3.47	4.34	5.63
	10^{-1}	1.38	1.72	2.24
	1	0.55	0.68	0.89
100	10^{-2}	6.59	8.47	11.1
	10^{-1}	2.62	3.37	4.41
	1	1.04	1.34	1.75
300	10^{-2}	16.6	23.2	31.6
	10^{-1}	6.59	9.22	12.6
	1	2.62	3.66	5.00
1000	10^{-2}	35.7	59.3	90.7
	10^{-1}	14.2	23.6	36.0
	1	5.63	9.36	14.3

Appendix B: Ratio of Kinetic Energy of Primary-Crater-Ejecta Mass to that of Original Meteorite

To derive for various primary-crater sizes an equation for calculating the ratio of the kinetic energy, E_S, of all primary-crater ejecta that impact beyond the continuous deposits and the original kinetic energy, E_0, of the meteorite, we first express the differential kinetic energy of fragments ejected from a primary crater and thrown to radial distance R in the satellitic crater field as

$$dE_S = dm_P \, V_S^2 \times 10^{10}/2 . \tag{B1}$$

For substitution into Equation (B1), we develop an expression for dm_P, as follows. First, we solve Equation (12) for the constant C and substitute the resulting expression into Equation (6) to obtain

$$dm_P = \frac{(b-2)\, m_e R^{1-b}\, dR}{1/R_0^{b-2} - 1/R_{\max}^{b-2}} , \tag{B2}$$

where we have assumed that $m_e = m_{PT}$. From Equation (A5), we find for a primary crater that

$$m_e = 3.2 \times 10^{-9} \, E_0 D_r^{-0.401} \cos^{1.134}\theta_0 , \tag{B3}$$

where the subscript 0 refers to the primary crater. Letting $D_r = 2R_r$ in Equation (B3) and substituting the result into Equation (B2), we obtain

$$dm_P = \frac{2.4 \times 10^{-9}\,(b-2)\, E_0 R_r^{-0.401} \cos^{1.134}\theta_0 R^{1-b}\, dR}{1/R_0^{b-2} - 1/R_{\max}^{b-2}} . \tag{B4}$$

Substitution of Equations (A7) and (B4) into Equation (B1) and integration of the resulting equation yield the ratio

$$\frac{E_S}{E_0} = \frac{34.8\,(b-2)\, R_r^{-0.401} \cos^{1.134}\theta_0}{1/R_0^{b-2} - 1/R_{\max}^{b-2}} \times \int_{R_{cd}}^{R\max} \left[\frac{\sin 2\theta_S}{2 \tan (R_S/3472)} + \sin^2 \theta_S \right]^{-1} R^{1-b}\, dR . \tag{B5}$$

Values of this ratio were calculated for various primary crater sizes by numerically integrating Equation (B5). In performing these calculations, it was assumed that the meteorite and fragments ejected from the primary crater impacted the lunar surface at angles of 45° and 75°, respectively, measured from the normal; i.e., $\theta_0 = 45°$ and $\theta_S = 75°$. Also, it was assumed that the fragments were ejected from the crater at a radial distance equal to $\frac{1}{2}$ the transient crater radius. A value of 3 was used for b, which is consistent with the value used previously in calculating m_{SC}/m_{PT}. In addition, the data of Short and Forman (1972) and of Baldwin (1963) were used to determine the values of R_0 in the case of crater slumping and of $R_{\max}$, respectively. The results, plotted in Figure 15, show that for all primary crater sizes considered, the kinetic

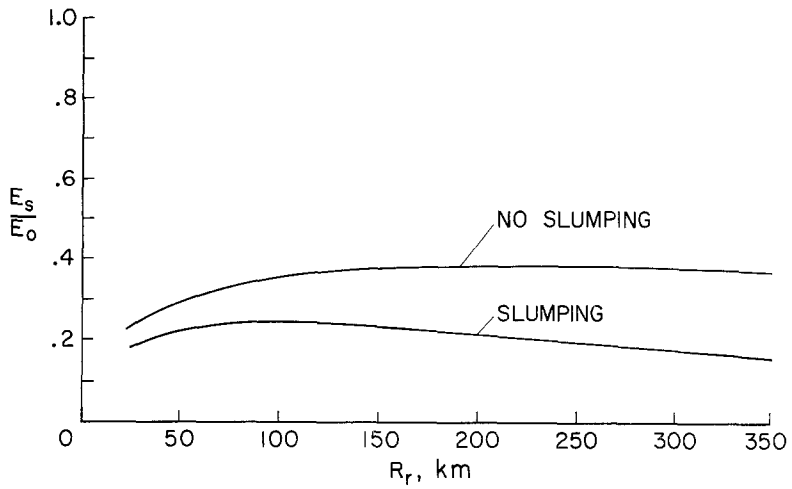

Fig. 15. Relative kinetic energy in the ejecta fragments that impacted outside the continuous deposit.

energy of the primary crater ejecta that impacts beyond the continuous deposits varies between 0.23 and 0.38 of the original meteorite's kinetic energy if crater slumping did not occur and between 0.16 and 0.24 if it did. Thus, the law of conservation of energy has not been violated.

Appendix C: Ratio of Cratering Efficiency of a Secondary Crater to that of a Primary Crater

Cratering efficiency is defined as the ratio of mass, m_e, ejected from a crater and the kinetic energy E, of the crater forming fragment. The ratio of cratering efficiency of a secondary crater and that of a primary crater can be derived from Equation (A5) of Appendix A as

$$\frac{(m_e/E)_S}{(m_e/E)_0} = \left(\frac{D_{r_0}}{D_{r_S}}\right)^{0.401} \left(\frac{\cos\theta_S}{\cos\theta_0}\right)^{1.134}, \tag{C1}$$

where D_{r_0} is primary-crater-rim diameter. If the impact angles for formation of a secondary crater and an 80-km-diameter primary crater are 75° and 45°, respectively, then the ratios of cratering efficiency of a secondary crater and cratering efficiency of a primary crater, calculated by using Equation (C1) are 48, 30, 12, and 4.7 for assumed secondary crater diameters of 0.3 m, 1 m, 10 m and 100 m, respectively. If both primary and secondaries are assumed to have been formed at the same impact angles then these values of efficiency ratios are increased by a factor of 3.12.

References

Adams, J. B. and McCord, T. B.: 1972, *Proc. Third Lunar Sci. Conf.* **3**, 3021–3034, MIT Press.
Adler, I., Trombka, J. I., Schmadebeck, R., Lowman, P., Blodget, H., Yin, L., Eller, E., Podwysocki,

M., Weidner, J. R., Bickel, A. L., Lum, R. K. L., Gerard, J., Gorenstein, P., Bjorkholm, P., and Harris, B.: 1973, *Proc. Fourth Lunar Sci. Conf.* **3**, 2783–2791, Pergamon Press.
Ahrens, T. J., O'Keefe, J. D., and Gibbons, R. V.: 1973, *Proc. Fourth Lunar Sci. Conf.* **3**, 2575–2590, Pergamon Press.
Baldwin, R. B.: 1963, *The Measure of the Moon*, Univ. of Chicago Press, Chicago, U.S.A.
Bence, A. E., Papike, J. J., Sueno, S., and Delano, J. W.: 1973, *Proc. Fourth Lunar Sci. Conf.* **1** 597–611, Pergamon Press.
Carlson, R. H. and Roberts, W. A.: 1963, *Project Sedan, PNI-217F*, The Boeing Co., Seattle, Wash., U.S.A.
Chao, E. C. T.: 1972, *J. Res. U.S. Geol. Surv.* **1**, 1–18.
Chao, E. C. T., Soderblom, L. A., Boyce, J. M., Wilhelms, D. E., and Hodges, C. A.: 1973, *Lunar Science IV* (Abstract), 127–128, The Lunar Sci. Inst., Houston, Tex., U.S.A.
Compston, W., Vernon, M. J., Chappell, B. W., and Freeman, R.: 1973, *Lunar Science IV* (abstract), 158.
Dence, M. R.: 1971, *J. Geophys. Res.* **76**, 5552–5565.
Dence, M. R. and Plant, A. G.: 1972, *Proc. Third Lunar Sci. Conf.* **1**, MIT Press, 379–399.
Dence, M. R., Grieve, R. A. F., and Plant, A. G.: 1974, *Lunar Science V*, 165–167, The Lunar Sci. Inst.
Eggleton, R. E. and Marshall, C. H.: 1962, *Astrogeolog. Studies Annual Progr. Rep., 1961*, U.S. Geol. Surv. 132–137.
Eggleton, R. E. and Schaber, G. G.: 1972, 'Cayley Formation Interpreted as Basin Ejecta', NASA SP-315, 29–7 through 29–16.
Elston, D. P., Boudette, E. L., Schafer, J. P., Muehlberger, W. R., and Sevier, J. R.: 1972, *Geotimes* **17**, 27–30.
Engelhardt, W. V.: 1971, *J. Geophys. Res.* **76**, 5566–5574.
Gault, D. E. and Wedekind, J.: 1973, unpublished data.
Gault, D. E. and Heitowit, E. D.: 1963, *Sixth Hypervelocity Impact Symposium*, Cleveland, Ohio. 2, pp. 419–456.
Gault, D. E., Quaide, W. L., and Oberbeck, V. R.: 1968, in Beven M. French and Nicholas M. Short (eds.), *Shock Metamorphism of Natural Materials*, Mono Book Corp., Baltimore, Md., pp. 87–99.
Hartmann, W. K. and Wood, C. A.: 1971, *The Moon* **3**, 3–78.
Hodges, C. A., Muehlberger, W. R., and Ulrich, G. E.: 1973, *Proc. Fourth Lunar Sci. Conf.* **1**, 1–25, Pergamon Press.
Howard, K. A.: 1973, *Science* **180**, 1052–1055.
Head, J. W.: 1973, *Trans. Am. Geophys. Union*, **54**, 1126–1129.
Head, J. W.: 1974, 'Stratigraphy of the Descartes Region (Apollo 16): Implications for the Origin of Samples', submitted to *The Moon*.
Husain, L. and Schaeffer, O. A.: 1973, *Lunar Science IV* (abstract), 406–408.
Hüttner, R.: 1969, *Geol. Bavarica* **61**, 142–200.
Johnson, S. W., Smith, J. A., Franklin, L. K., Horaski, L. K., and Teal, D. J.: 1969, *J. Geophys. Res.* **74**, 4838.
Kieffer, S. W.: 1971, *J. Geophys. Res.* **76**, 5449–5473.
LSPET (Lunar Sample Preliminary Examination Team): 1973, *Science* **179**, 23–34.
Marcus, A. H.: 1968, *Covariance Function of Elevations on a Cratered Planetary Surface*, Part II, TR-68-340-5, Bellcomm, Inc.
McCord, T. B., Charette, M. P., Johnson, T. V., Lebofsky, L. A., and Pieters, C.: 1972a, *J. Geophys. Res.* **77**, 1349–1359.
McCord, T. B., Charette, M. P., Johnson, T. V., Lebofsky, L. A., and Pieters, C.: 1972b, *The Moon* **5**, 52–89.
McGetchin, T. R., Settle, M., and Head, J. W.: 1973, *Earth Planetary Sci. Letters* **20**, 226–236.
Milton, D. J.: 1972, 'Geologic Map of the Descartes Region of the Moon', Apollo 16 Premission Map, *U.S. Geol. Surv. Misc. Geol. Inv. Map I-748*.
Morris, E. C. and Wilhelms, D. E.: 1967, 'Geologic Map of the Julius Caesar Quadrangle of the Moon', I-510 (LAC 60), *U.S. Geol. Surv.* Washington, D.C., U.S.A.
Mutch, T. A.: 1972, *Geology of the Moon*, Princeton Univ. Press, Princeton, N.J.
Oberbeck, V. R.: 1971a, *The Moon* **2**, 263–278.
Oberbeck, V. R.: 1971b, *J. Geophys. Res.* **76**, 5732–5749.

Oberbeck, V. R. and Morrison, R. H.: 1973, *Proc. Fourth Lunar Sci. Conf.* **1**, 107–123, Pergamon Press.

Oberbeck, V. R. and Morrison, R. H.: 1974, *The Moon* **9**, 415–455.

Pearce, G. W., Gose, W. A., and Strangway, D. W.: 1973, *Proc. Fourth Lunar Sci. Conf.* **3**, 3045–3076, Pergamon Press.

Pohn, H. A.: 1972, 'Geologic Map of the Tycho Quadrangle of the Moon', I-713 (LAC 112), *U.S. Geological Survey*, Washington, D.C., U.S.A.

Pohn, H. A. and Wildey, R. L.: 1970, 'A Photoelectric-Photographic Study of the Normal Albedo of the Moon', *U.S. Geol. Surv. Prof. Paper 599-E.*

Shoemaker, E. M.: 1962, in Z. Kopal (ed.), *Physics and Astronomy of the Moon*, Academic Press, New York, N.Y., U.S.A., pp. 283–359.

Shoemaker, E. M.: 1963, in B. M. Middlehurst and G. P. Kuiper (eds.), *The Moon, Meteorites and Comets*, p. 301, Univ. of Chicago Press.

Short, N. M. and Forman, M. L.: 1972, *Modern Geol.* **3**, 69–91.

Soderblom, L. A. and Boyce, J. M.: 1972, 'Relative Ages of Some Nearside and Farside Terra Plains Based on Apollo 16 Metric Photography', *Apollo 16 Preliminary Science Report*, NASA SP-315, 29-3 through 29-6.

Soderblom, L. A. and Lebofsky, L. A.: 1972, *J. Geophys. Res.* **77**, 279.

Teller, E., Talley, W. K., Higgins, G. H., and Johnson, G. W.: 1968, *The Constructive Uses of Nuclear Explosives*, McGraw-Hill Book Co., N.Y., pp. 146–147.

Tera, F., Papanastassiou, D. A., and Wasserburg, G. J.: 1973, *Lunar Science IV* (abstract), 723–725.

Trask, N. J. and McCauley, J. F.: 1972, *Earth Planetary Sci. Letters* **14**, 201–206

Trombka, J. I., Arnold, J. R., Reedy, G. C., Peterson, L. E., and Metzger, A. E.: 1973, *Proc. Fourth Lunar Sci. Conf., Suppl. 4, Geochim. Cosmochim. Acta* **3**, 2847–2853.

Ulrich, G. E.: 1973, *Proc. Fourth Lunar Sci. Conf.* **1**, 27–39, Pergamon Press.

Walker, D., Longhi, J., and Hays, J. F.: 1973, *Lunar Science IV* (abstract), 752–754.

Warner, J. L., Simonds, C. H., and Phinney, W. C.: 1973, *Proc. Fourth Lunar Sci. Conf.* **1**, 481–504, Pergamon Press.

Whitaker, E. A.: 1972, *Apollo 16 Preliminary Science Report*, NASA SP-315, 29–39.

Wilhelms, D. E.: 1965, 'Astrogeological Studies Annual Progress Report, 1964–65', *U.S. Geol. Surv.* 13–28.

Wilhelms, D. E.: 1968, 'Geologic Map of The Mare Vaporum Quadrangle of the Moon', I 548 (LAC59), *U.S. Geol. Surv.*, Washington, D.C., U.S.A.

Wilhelms, D. E. and McCauley, J. F.: 1971, 'Geologic Map of the Near Side of the Moon', *U.S. Geol. Surv. Misc. Geol. Inv. Map I-703.*

Wilshire, H. G., Stuart-Alexander, D. E., and Jackson, E. D.: 1973, *J. Geophys. Res.* **78**, 2379–2392.